Title

Amplification of oncolytic vaccinia virus widespread tumor cell killing by sunitinib through multiple mechanisms

Journal

Cancer Research, 78(4)

ISSN

0008-5472

Authors

Kim, Minah
Nitschké, Maximilian
Sennino, Barbara
et al.

Publication Date

2018-02-15

DOI

10.1158/0008-5472.can-15-3308

Peer reviewed

Published OnlineFirst December 19, 2017; DOI: 10.1158/0008-5472.CAN-15-3308

Tumor Biology and Immunology

Cancer Research

Amplification of Oncolytic Vaccinia Virus Widespread Tumor Cell Killing by Sunitinib through Multiple Mechanisms

Minah Kim[1], Maximilian Nitschké[1], Barbara Sennino[1], Patrizia Murer[1], Brian J. Schriver[1], Alexander Bell[1], Aishwarya Subramanian[1], Corry E. McDonald[1], Jiahu Wang[2], Howard Cha[1], Marie-Claude Bourgeois-Daigneault[2], David H. Kirn[3], John C. Bell[2], Naomi De Silva[3], Caroline J. Breitbach[3], and Donald M. McDonald[1]

Abstract

Oncolytic viruses pose many questions in their use in cancer therapy. In this study, we assessed the potential of mpJX-594 (mouse-prototype JX-594), a replication-competent vaccinia virus administered by intravenous injection, to target the tumor vasculature, produce immune activation and tumor cell killing more widespread than the infection, and suppress invasion and metastasis. These actions were examined in RIP-Tag2 transgenic mice with pancreatic neuroendocrine tumors that developed spontaneously and progressed as in humans. mpJX-594 initially infected tumor vascular endothelial cells, leading to vascular pruning and prolonged leakage in tumors but not in normal organs; parallel effects were observed in U87 gliomas. Viral infection spread to tumor cells, where tumor cell killing was much more widespread than the infection. Widespread tumor cell killing at 5 days was prevented by depletion of $CD8^+$ T lymphocytes and did not require GM-CSF, as mpJX-594 variants that expressed human, mouse, or no GM-CSF produced equivalent amounts of killing. The antivascular, antitumor, and antimetastatic effects of mpJX-594 were amplified by concurrent or sequential administration of sunitinib, a multitargeted receptor tyrosine kinase inhibitor. These effects were not mimicked by selective inhibition of VEGFR2 despite equivalent vascular pruning, but were accompanied by suppression of regulatory T cells and greater influx of activated $CD8^+$ T cells. Together, our results showed that mpJX-594 targets tumor blood vessels, spreads secondarily to tumor cells, and produces widespread $CD8^+$ T-cell–dependent tumor cell killing in primary tumors and metastases, and that these effects can be amplified by coadministration of sunitinib.

Significance: These findings reveal multiple unrecognized features of the antitumor properties of oncolytic vaccinia viruses, all of which can be amplified by the multitargeted kinase inhibitor sunitinib. *Cancer Res; 78(4); 922–37. ©2017 AACR.*

Introduction

Replication-competent oncolytic viruses that selectively infect tumors are emerging as a novel class of cancer therapeutics (1–5). JX-594 (Pexa-Vec, *pexastimogene devacirepvec*) is a vaccinia vaccine-derived oncolytic poxvirus engineered to inactivate viral thymidine kinase (TK) and express transgenes encoding human granulocyte-macrophage colony-stimulating factor (hGM-CSF, encoded by CSF2) as an immune response promoter and β-galactosidase as a reporter (6–9).

JX-594 and related oncolytic viruses are designed to induce direct oncolysis and immune-mediated killing of tumor cells (10–15). Oncolytic viruses induce immune responses not only against viral antigens but also against tumor antigens and can thereby target noninfected metastases (5, 11, 13, 14). The respective contributions of oncolysis and immunologically mediated tumor cell death are now being elucidated (15).

Oncolytic viruses can also target and disrupt the tumor vasculature (16–19). Consistent with their antivascular effects, the antitumor actions of oncolytic viruses are influenced by antiangiogenic agents, but the effects vary with the treatment regimen and have different underlying mechanisms. Administration of anti-VEGF antibody concurrently with vaccinia virus strongly reduces viral infection of tumors, suggestive of an essential role of VEGF signaling on viral tropism to tumor blood vessels (20). However, brief pretreatment with anti-VEGF antibody or the angiogenesis inhibitor sunitinib increases the antitumor effect of reovirus, reportedly because withdrawal of the inhibitor triggers a rebound burst of VEGF that increases endothelial cell infection, vascular disruption, and viral delivery to tumor cells (21). Pretreatment with recombinant VEGF has similar effects (21). By a different experimental approach, sunitinib was found to amplify the antitumor effects of vaccinia virus when administered 7 days after the virus but not when given 7 days before (19).

[1]UCSF Helen Diller Family Comprehensive Cancer Center, Cardiovascular Research Institute and Department of Anatomy, University of California, San Francisco, San Francisco, California. [2]Centre for Innovative Cancer Therapeutics, Ottawa Hospital Research Institute, Ottawa, Ontario, Canada. [3]SillaJen Biotherapeutics Inc., San Francisco, California.

Note: Supplementary data for this article are available at Cancer Research Online (http://cancerres.aacrjournals.org/).

M. Kim, M. Nitschké, and B. Sennino contributed equally to this article.

Corresponding Author: D.M. McDonald, University of California, San Francisco, 513 Parnassus Avenue, Room S1349, San Francisco, CA 94143-0452. Phone: 415-476-2118; Fax: 415-502-0418; E-mail: donald.mcdonald@ucsf.edu

doi: 10.1158/0008-5472.CAN-15-3308

Published OnlineFirst December 19, 2017; DOI: 10.1158/0008-5472.CAN-15-3308

Prolongation of virally induced vascular collapse and suppression of angiogenesis were the presumptive mechanisms (19).

Complicating the interpretation of these experiments, sunitinib has immune-modulatory effects in addition to antivascular actions when given with oncolytic viruses (14). Sunitinib decreases regulatory T cells (Treg) and myeloid-derived suppressor cells (MDSC) in some tumors (22–24). Sunitinib also promotes replication of oncolytic vesicular stomatitis virus in tumors by inhibiting innate antiviral immunity (25).

Building on this background, we sought to determine (i) the location of infection after intravenous administration of oncolytic virus and the temporal sequence of spread from tumor blood vessels to tumor cells; (ii) whether regions of tumor cell death extend beyond sites of infection in tumors; (iii) whether tumor cell killing beyond sites of infection depends on cytotoxic $CD8^+$ T-cell influx; (iv) whether this initial tumor cell killing requires viral GM-CSF expression; and (v) whether effects of sunitinib on tumor vascularity, leakiness, or immune modulation promote virally mediated tumor cell killing through a VEGFR2–dependent mechanism.

We addressed these issues by examining the effects of mpJX-594 in RIP-Tag2 transgenic mice, which spontaneously develop insulinomas (pancreatic neuroendocrine tumors, PNET) in their natural location (26). The tumors manifest multiple stages of progression and are highly responsive to angiogenesis inhibitors (27, 28). mpJX-594 is a Western Reserve strain of vaccinia virus, which, like its clinical counterpart JX-594/Pexa-Vec, has viral TK inactivation and expresses human GM-CSF (18, 29).

Anti-CD8 antibody was administered with mpJX-594 over 5 days to determine whether the initial widespread tumor cell killing by the virus was dependent on cytotoxic $CD8^+$ T cells. With the understanding that human GM-CSF has limited activity in mice (30, 31), we compared three mpJX-594 variants, which expressed human GM-CSF, mouse GM-CSF, or no GM-CSF, to determine whether viral GM-CSF made a significant contribution to the widespread tumor cell killing found at 5 days. The experiment was designed to match the other 5-day experiments, with recognition that the production and downstream effects of viral GM-CSF probably take longer than 5 days to peak. Antiangiogenic effects were assessed by comparing mpJX-594 alone and together with sunitinib (32) or anti-VEGFR2 antibody DC101 (33).

Experiments revealed that i.v. administration of mpJX-594 was rapidly followed by selective infection of tumor vascular endothelial cells, loss of endothelial barrier function, and reduction in tumor vascularity. The viral infection spread to focal regions of tumor cells. Apoptosis was extensive at 5 days and was much more widespread than the viral infection. Cell killing beyond infected regions of tumors at 5 days was dependent on $CD8^+$ T-cell influx but not on viral GM-CSF expression. The antivascular, antitumor, and antimetastatic effects of mpJX-594 were amplified by sunitinib, independent of administration sequence. These actions of sunitinib were not explained by vascular pruning and were not mimicked by VEGFR2 inhibition by DC101, but were accompanied by suppression of Tregs and greater influx of $CD8^+$ T cells.

Materials and Methods

Oncolytic viruses and tumor cell lines

Variants of mpJX-594 vaccinia virus used for studies in RIP-Tag2 transgenic mice were generated from the Western Reserve strain (WR). WR is a Wyeth strain vaccinia virus isolated through serial passage in mice to select for replication in mouse cells (34). A cassette containing enhanced GFP or yellow fluorescent protein (YFP) and GM-CSF or mCherry transgenes under the synthetic early/late promoter (pSE/L) was inserted into the vaccinia TK gene locus, thereby inactivating TK gene function (Supplementary Fig. S1A–S1C). Three variants of mpJX-594 that express human GM-CSF (mpJX-594/hGM-CSF), mouse GM-CSF (mpJX-594/mGM-CSF), or mCherry instead of GM-CSF (mpJX-594/mCherry) were created (Supplementary Fig. S1A–S1C). The variant expressing hGM-CSF (also designated mpJX-594) was used unless otherwise specified. All three variants were used to determine the contribution of GM-CSF to the antitumor action of mpJX-594. mpJX-594/mCherry lacking GM-CSF was also used in studies of 4T1 mouse mammary carcinomas in syngeneic BALB/c mice. The clinical vaccinia virus JX-594, propagated in U2OS cells, was used in studies of human U87 gliomas in nude mice. JX-594 is a Wyeth vaccinia vaccine-derived oncolytic virus modified by inactivation of the viral TK gene by insertion of hGM-CSF and β-galactosidase transgenes under control of the synthetic early-late and p7.5 promoters, respectively (35). U87 and 4T1 tumor cell lines were obtained from the ATCC, authenticated by short tandem repeat analysis or direct sequencing, and tested for mycoplasma contamination and found to be negative.

Tumor models and treatments

Tumor-bearing RIP-Tag2 transgenic mice (C57BL/6 background) at age 13 weeks received mpJX-594/hGM-CSF, mpJX-594/mGM-CSF, or mpJX-594/mCherry (10^7 pfu in 100 μL of PBS) by tail vein injection on day 0 and were studied 5 days later in most experiments. Time-course studies also examined 6 hours, 1 day, and 2 days after mpJX-594. Dose-response studies compared effects of the standard 10^7 pfu dose of mpJX-594/mGM-CSF with 3 or 6 times this dose at 5 days. In $CD8^+$ T-cell depletion experiments, RIP-Tag2 mice received 400 μg anti-CD8 antibody (Clone 2.43) or control IgG (Rat, Clone LTF-2, both BioXCell) in 100 μL i.p. on days −2, −1, 1, and 3. Virus was injected at day 0. Mice were studied on day 5.

In experiments of angiogenesis inhibitors, mice received sunitinib (40 mg/kg in 5 μL/g sterile saline with 0.5% methylcellulose suspension, Pfizer) by gavage daily alone or with mpJX-594. Relevance of the sequence of administration of one dose mpJX-594 and daily sunitinib over 10 days was tested by giving both agents together or by giving one or the other agent alone 5 days before starting the second agent. Effects of 30-day treatment with mpJX-594 and/or sunitinib were examined by injecting mpJX-594/hGM-CSF on days 0 and 15 and giving sunitinib daily on days 5 to 29. The contribution of VEGF signaling blockade to the effects of sunitinib was tested with the selective VEGFR2 inhibitor DC101 antibody (Monoclonal Antibody Core), 40 mg/kg i.p. twice over 5 days, with or without a priming dose (100 mg/kg i.p.) the day before injection of mpJX-594. Controls were treated with vehicle (PBS).

U87 human glioblastoma cells (1×10^6 U87MGvIII cells; ATCC) were implanted subcutaneously on both flanks of CD1 athymic nude mice at age 6 to 8 weeks. The clinical vaccinia virus JX-594 (10^8 pfu) was injected i.v. approximately 2 weeks after implantation. Tumors were studied 6 hours to 5 days thereafter.

4T1 mouse mammary carcinoma cells (2×10^5 4T1 cells; ATCC) were implanted subcutaneously in syngeneic BALB/c mice at age 6 to 8 weeks. Twelve days after implantation (designated

Published OnlineFirst December 19, 2017; DOI: 10.1158/0008-5472.CAN-15-3308

day 0), mice received a single i.v. dose of vehicle or mpJX-594/mCherry (5×10^7 pfu), the first of 5 daily doses of sunitinib (20 mg/kg) by gavage, or a combination of the two treatments. Tumors were removed 5 days after the onset of treatment.

Mice were housed under barrier conditions in the animal care facility at the University of California, San Francisco (UCSF) or Ottawa Hospital Research Institute. All experimental procedures were approved by the Institutional Animal Care and Use Committees.

Tissue preparation, immunohistochemistry, and measurements

After treatment, mice were anesthetized (ketamine 87 mg/kg and xylazine 13 mg/kg by intramuscular injection), and tissues were preserved by vascular perfusion of fixative (1% paraformaldehyde in PBS; refs. 28, 36). Cryostat sections 80-μm in thickness were stained immunohistochemically for viral antigen (vaccinia), mpJX-594 viral replication (YFP), tumor vascularity (CD31 or VEGFR2), tumor cells (SV40 T-antigen or insulin), acinar pancreas (amylase), apoptosis (activated caspase-3), leukocytes (CD45 or CD8), or extravasated erythrocytes (TER119; refs. 28, 36). Some mice received 50-nm microspheres (50 μL i.v., Dragon Green, Bangs Laboratories Inc.) before anesthesia to assess vascular leakage. Mice were anesthetized 7 minutes later. Intravascular microspheres were removed by fixative perfusion at 10 minutes. Specimens were examined with a Zeiss Axiophot fluorescence microscope and Zeiss LSM 510 laser scanning confocal microscope (36). Amounts of immunohistochemical staining and microsphere extravasation were measured with ImageJ (http://imagej.nih.gov/ij/; ref. 36). Supplementary Methods have more information on methods for histochemical staining and measurements of tumor.

Flow cytometry

Cells isolated from collagenase-digested RIP-Tag2 tumors were stained for CD45, CD3e, CD4, and CD8 and analyzed by flow cytometry. Activated $CD8^+$ T cells were identified by granzyme B staining, and Tregs were identified by Foxp3 staining after permeabilization. Supplementary Methods have details of methods for flow cytometry.

Statistical analysis

Values are expressed as mean ± SEM for 5 mice per group, unless indicated otherwise in figure legends. Differences were assessed by the Student *t* test or ANOVA followed by Tukey test for multiple comparisons (Prism 6, Graphpad), where $P < 0.05$ was considered significant. Differences in metastasis incidence were assessed by the Fisher exact test (R, version 3.4.1), where $P < 0.05$ was considered significant.

Results

mpJX-594 viral replication in RIP-Tag2 tumors

Vaccinia immunoreactivity was absent in tumors of 13-week-old RIP-Tag2 mice treated with vehicle control (Supplementary Fig. S2A and S2B) but was visible as faint staining in most blood vessels in tumors 6 hours after i.v. injection of mpJX-594. No staining was found in tumor cells or other cells outside the vasculature at 6 hours (Supplementary Fig. S2A and S2B). At 1 day, vaccinia was visible in most tumor blood vessels and in focal extravascular regions confluent with tumor vessels (Supplementary Fig. S2A and S2B). The amount and brightness of vaccinia staining were greater at 5 days when discrete clusters of vaccinia-positive cells were visible in most tumors (Supplementary Fig. S2A and S2B). YFP, which required viral replication for expression (Supplementary Fig. S1), had a similar distribution (Supplementary Fig. S2C and S2D), confirming that staining for vaccinia reflected sites of active infection rather than sequestration of virus.

Spleen and liver of RIP-Tag2 mice were tested for vaccinia and YFP staining to determine whether mpJX-594 entered and replicated in cells outside tumors (Supplementary Fig. S3). Vaccinia staining in the spleen was strong at 6 hours but was faint at 1 day and absent at 5 days (Supplementary Fig. S3A). The significance of the strong vaccinia staining in the spleen at 6 hours was assessed by YFP staining. Little or no YFP was found at 6 hours or other times (Supplementary Fig. S3B). Although faint vaccinia staining was evident in liver sinusoids at 6 hours, none was found at 5 days, and no YFP fluorescence was detected at either time (Supplementary Fig. S3C).

mpJX-594 effects on tumor vasculature, tumor cells, and tumor burden

Blood vessels in RIP-Tag2 tumors became progressively more leaky from 6 hours to 5 days after i.v. injection of mpJX-594. At 10 minutes after i.v. injection, extravasated 50-nm microspheres were limited to small, scattered regions of control tumors, but were widespread in tumors at 5 days after mpJX-594, indicative of sustained blood flow and leakage (Fig. 1A and B).

Like microspheres, extravasation of fibrinogen/fibrin and erythrocytes requires blood flow, endothelial barrier defects, and transmural driving force, but unlike microspheres, intratumoral fibrin and hemorrhage provide historical records of leakage (37–39). Fibrin had a patchy distribution in control tumors (39), but at 5 days after mpJX-594, fibrin outlined the vasculature and filled scattered regions in tumors (Supplementary Fig. S4A). Fibrin was 161% more widespread at 5 days after mpJX-594 than in tumors of littermate controls (Fig. 1C).

Similar differences were found in extravasated erythrocytes, which in control tumors had a patchy distribution similar to that of fibrin (Supplementary Fig. S4B; refs. 38, 39). At 5 days after mpJX-594, extravasated erythrocytes were more than twice as abundant as in control tumors (Fig. 1C), consistent with a sustained endothelial barrier defect.

mpJX-594 infection was accompanied by vascular pruning in tumors (Fig. 1D). Tumor vascularity assessed by CD31 staining was reduced by 37% at 5 days after mpJX-594 (Fig. 1E). To test whether CD31 staining faithfully reflected tumor vascularity, tumor blood vessels were costained for CD31 and VEGFR2 after vehicle or mpJX-594 (5 days). CD31 and VEGFR2 measurements were equal at baseline and similarly decreased after mpJX-594 (Supplementary Fig. S4C and S4D).

At 5 days after mpJX-594, most vaccinia staining was in discrete clusters (Fig. 1D and F). By comparison, apoptosis shown by staining for activated caspase-3 was much more widespread. Apoptotic cells were sparse and scattered in vehicle-treated tumors, but were abundant and widely distributed after mpJX-594 (Fig. 1G). On average, the amount of activated caspase-3 staining was about 8-fold the amount of vaccinia (38% vs. 5%; Fig. 1F and H). Consistent with the large increase in cell death, tumors in mice at 5 days after mpJX-594 were significantly smaller than controls (Fig. 2A).

Published OnlineFirst December 19, 2017; DOI: 10.1158/0008-5472.CAN-15-3308

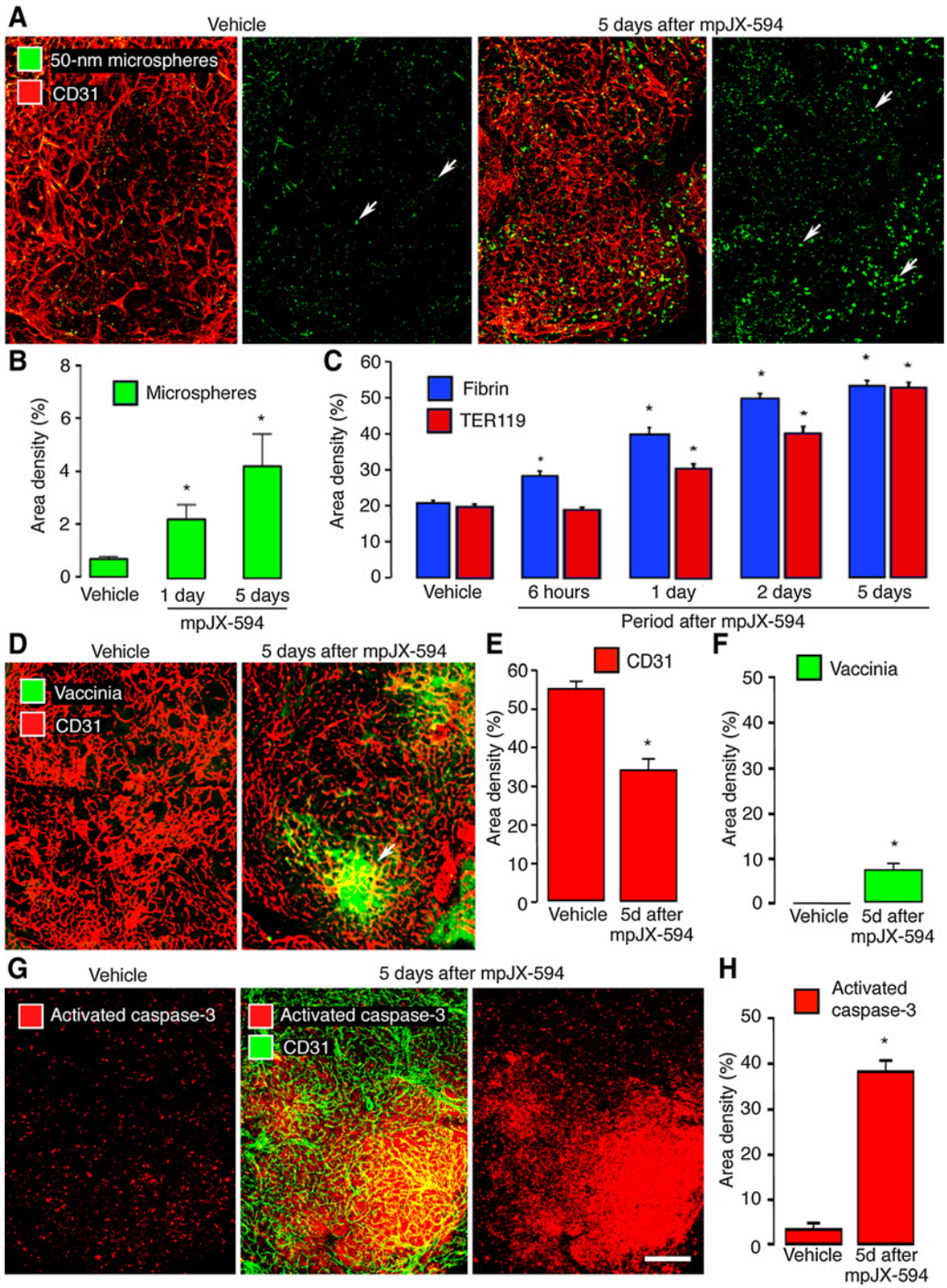

Figure 1.

mpJX-594 effects on vascular leakage and tumor cell killing. **A,** Extravasated 50-nm microspheres (green), shown with blood vessels (CD31, red) and alone in RIP-Tag2 tumors, are sparse at 5 days after vehicle but are abundant after mpJX-594. **B,** Microsphere extravasation was greater at 5 days than at 1 day after mpJX-594. ANOVA: *, $P < 0.05$ compared with vehicle ($n = 4$ mice/group). **C,** Time-dependent increase in staining for extravasated fibrin (blue) and erythrocytes (TER119, red) in tumors from 6 hours to 5 days after i.v. injection of mpJX-594. ANOVA: *, $P < 0.05$ for difference compared with vehicle for 5 days ($n = 5$ mice/group). **D,** Confocal micrographs of blood vessels (CD31, red) and vaccinia staining (green, arrow) in RIP-Tag2 tumors at 5 days after one dose of vehicle or mpJX-594. **E** and **F,** Differences in tumor vascularity (CD31 staining) and vaccinia staining at 5 days after vehicle or mpJX-594. *, $P < 0.05$ compared with vehicle ($n = 5$ mice/group). **G,** Confocal micrographs of apoptotic cells (activated caspase-3, red) stained alone and with blood vessels (CD31, green) in RIP-Tag2 tumors at 5 days after vehicle or mpJX-594. **H,** Large increase in activated caspase-3 staining at 5 days after mpJX-594. ANOVA: *, $P < 0.05$ compared with vehicle ($n = 5$ mice/group). Scale bar in **G** applies to all images, 200 μm.

Published OnlineFirst December 19, 2017; DOI: 10.1158/0008-5472.CAN-15-3308

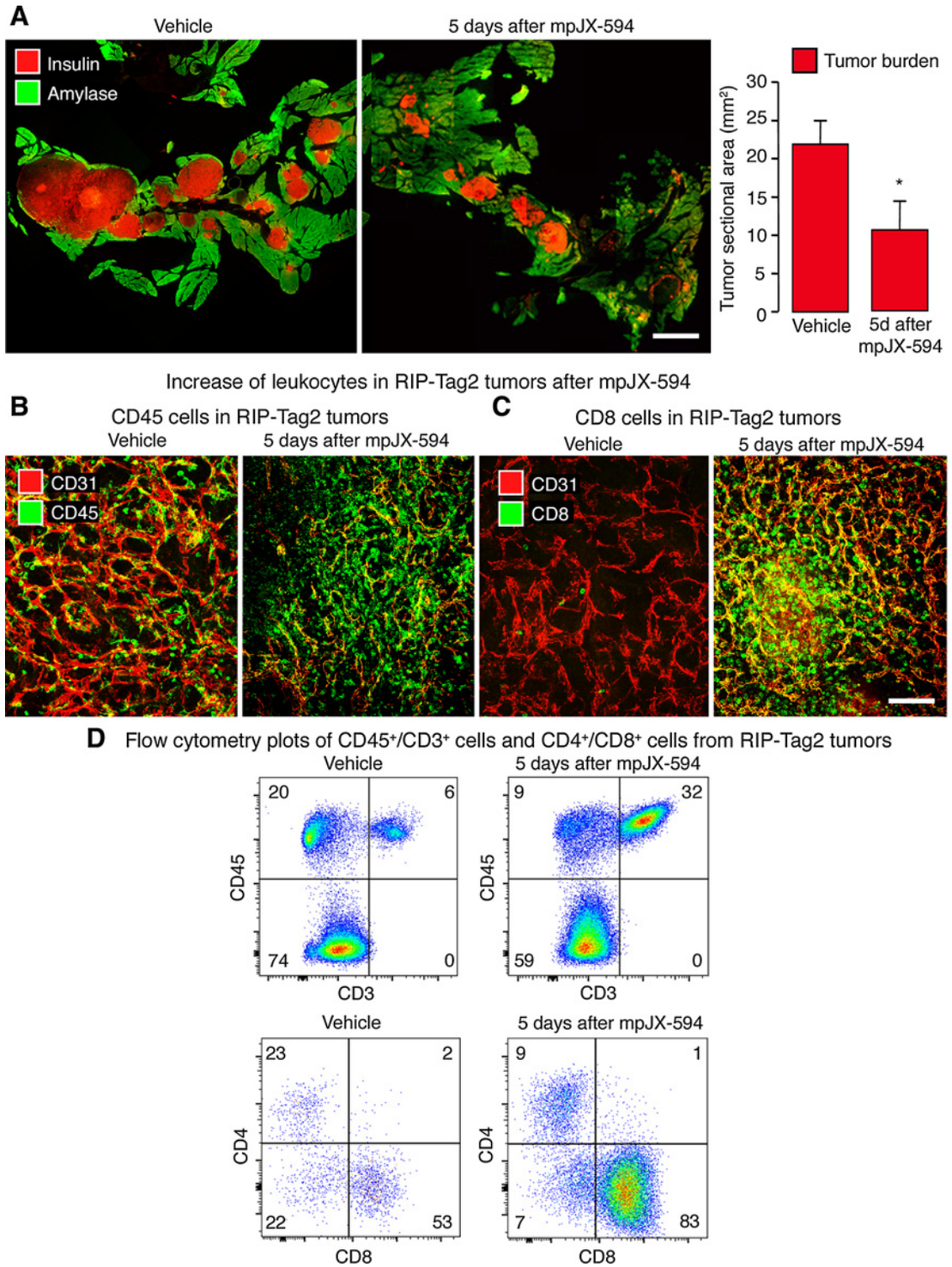

Figure 2.

mpJX-594 effects on tumor burden and leukocyte influx. **A,** Tumor size indicated by staining of tumor cells for insulin (red) and pancreatic acinar cells for amylase (green) at 5 days after one dose of vehicle (left) or mpJX-594 (right). Graph shows corresponding measurements of tumor burden estimated as combined area of all tumors in sections of pancreas (see Materials and Methods). Student *t* test: *, $P < 0.05$ compared with vehicle ($n = 5$ mice/group). **B,** Confocal micrographs of leukocytes (CD45, green) and blood vessels (CD31, red) in RIP-Tag2 tumors at 5 days after vehicle or mpJX-594. **C,** Confocal micrographs show greater abundance of $CD8^+$ T cells (green) in tumors after mpJX-594. Blood vessels, CD31, red. **D,** Flow cytometry plots of $CD45^+/CD3^+$ cells (from all living cells in tumor) and $CD4^+/CD8^+$ cells (from $CD45^+/CD3^+$ fraction) isolated from tumors show increases in $CD3^+$ cells and $CD8^+$ cells (percentages in corners) at 5 days after mpJX-594. Scale bar, 3 mm in **A** and 100 μm in **C**.

Published OnlineFirst December 19, 2017; DOI: 10.1158/0008-5472.CAN-15-3308

mpJX-594 effects on CD8$^+$ T-cell influx

We next determined whether the extent and distribution of tumor cell killing after mpJX-594 were governed by cytotoxic CD8$^+$ T cells. Although CD45$^+$ leukocytes were numerous in RIP-Tag2 tumors even in the absence of mpJX-594 (Fig. 2B), CD8$^+$ T cells were sparse in control tumors but were very abundant after mpJX-594 (Fig. 2C). Flow cytometry of CD45$^+$ cells dissociated from RIP-Tag2 tumors confirmed that CD3$^+$ T cells increased after mpJX-594 and that CD8$^+$ T cells were the dominant population (Fig. 2D).

The contribution of cytotoxic T cells to the antitumor effects of mpJX-594 in RIP-Tag2 mice was tested by giving the virus after depletion of CD8$^+$ T cells with anti-CD8$^+$ antibody for 5 days. Depletion was confirmed by immunohistochemistry and flow cytometry (Fig. 3A and B). CD8$^+$ T-cell depletion had little effect on the amount and distribution of vaccinia staining in tumors (Fig. 3C and D). However, tumor cell apoptosis marked by activated caspase-3 staining was significantly reduced in tumors after depletion of CD8$^+$ T cells and had a strikingly different distribution (Fig. 3E and F). Apoptosis in tumors after mpJX-594 in mice lacking CD8$^+$ T cells was limited to focal regions of vaccinia staining, unlike the widespread distribution in tumors of mice with intact CD8$^+$ T cells (Fig. 3C–F).

Contribution of GM-CSF from mpJX-594 to tumor cell killing

To determine the contribution of viral GM-CSF expression to the initial widespread tumor cell killing by mpJX-594, we compared the amount of tumor-cell apoptosis at 5 days after three viral variants, which expressed human GM-CSF, mouse GM-CSF, or no GM-CSF (Supplementary Fig. S1). Activated caspase-3 staining in tumors was 48- to 53-fold greater than the baseline (vehicle) after all variants of mpJX-594, and no differences were found among the three variants (Supplementary Fig. S5A and S5B), indicative of limited contribution of viral GM-CSF at 5 days. A dose-response study revealed that a 6-fold dose of mpJX-594/mGM-CSF was accompanied by only doubling of activated caspase-3 staining at 5 days (Supplementary Fig. S5C). Consistent with other experiments, activated caspase-3 staining was significantly greater than vaccinia staining at all three doses (Supplementary Fig. S5C).

JX-594 effects on U87 gliomas

To test the effects of the virus in another tumor model, we performed similar experiments using JX-594 in mice with U87 gliomas. As in RIP-Tag2 tumors, vaccinia staining was absent in the controls, was found near tumor vessels at 6 hours after JX-594, was in scattered tumor cells at 1 day, and was widespread in tumors at 5 days (Supplementary Fig. S6A). Extravasated fibrin, as an indicator of defective endothelial barrier function, was sparse in control U87 tumors, but outlined tumor vessels at 1 day after JX-594 and was widely distributed in tumors at 5 days (Supplementary Fig. S6B). Activated caspase-3 was sparse in control tumors but was abundant near tumor vessels at 1 day after JX-594 (Supplementary Fig. S6C). After JX-594, tumor vessels were narrower, and tumor vascularity was reduced 30% at 1 day, 38% at 2 days, and 56% at 5 days (Supplementary Fig. S6D and S6E).

mpJX-594 plus sunitinib: Amplified antitumor effects

As sunitinib has been shown to increase the antitumor action of some oncolytic viruses (19), we compared the effects of mpJX-594 and sunitinib given individually or together to RIP-Tag2 mice. Amounts of vaccinia infection, vascular pruning and leakage, and tumor cell killing were used as readouts.

Vaccinia staining in tumors after mpJX-594 plus sunitinib was nearly 5-fold the amount after mpJX-594 alone (34% vs. 7%; Fig. 4A and B). The decrease in tumor vascularity was also greater at 5 days after the combination (55% reduction) than after mpJX-594 (37% reduction) or sunitinib alone (36% reduction; Fig. 4C). Extravasation of 50-nm microspheres was >60% greater at 1 and 5 days after mpJX-594 plus sunitinib than after mpJX-594 alone (Fig. 4D and E). Microsphere leakage after the combination was 5 times the baseline at 1 day and 10 times the baseline at 5 days (Fig. 4E). Leakage after sunitinib was similar to the control at both times (Fig. 4E). Sustained leakage after the combination of agents indicated that sunitinib did not result in tumor vessel normalization with suppression of leakage under these conditions (38).

Greater vaccinia infection after mpJX-594 plus sunitinib was accompanied by more uniform and widespread apoptosis in RIP-Tag2 tumors (Fig. 4F and G). Activated caspase-3 staining was 17-fold the baseline value when the two agents were given together, compared with 10-fold after mpJX-594 alone and 2-fold after sunitinib alone (Fig. 4G). The disproportionate increase in activated caspase-3 compared with the reduction in tumor vascularity after mpJX-594 plus sunitinib (Fig. 4C and G) argues against the antiangiogenic action of sunitinib as the main mechanism of amplification of tumor cell killing.

Sunitinib amplification of mpJX-594-induced tumor cell killing was similar at 5 days regardless of whether the virus expressed human or mouse GM-CSF. Tumors in RIP-Tag2 mice given mpJX-594/mGM-CSF plus sunitinib had significantly more activated caspase-3 at 5 days than after the virus alone (Supplementary Fig. S7A and S7B), and the amount of amplification was about the same as found with mpJX-594/hGM-CSF (Fig. 4G).

Tumor burden in RIP-Tag2 mice treated with mpJX-594/hGM-CSF plus sunitinib for 5 days fit with the widespread tumor cell killing. Tumor burden in mice treated with both agents was less than half the value of mice treated with mpJX-594 or sunitinib alone and only 20% of vehicle-treated controls (Fig. 4H).

mpJX-594 plus sunitinib: Effects on 4T1 mammary carcinomas

4T1 mouse mammary carcinomas were implanted in syngeneic BALB/c mice to test whether coadministration of sunitinib increased the antitumor effect of mpJX-594 on these tumors over 5 days as found in RIP-Tag2 tumors (Supplementary Fig. S7C). 4T1 tumors treated with mpJX-594/mCherry (no GM-CSF expressed) plus sunitinib were significantly smaller (57% reduction) than the controls. Neither the virus nor sunitinib given alone resulted in consistent growth slowing under these conditions (Supplementary Fig. S7C).

mpJX-594 plus sunitinib: Effects on immune response

As sunitinib can influence the action of oncolytic viruses through effects on innate and adaptive immunity (14, 22, 25), we examined this issue in RIP-Tag2 tumors. CD45$^+$ cells and CD8$^+$ T cells were much more abundant in tumors in mice treated with mpJX-594 plus sunitinib than in untreated tumors (Fig. 5A and B). Flow cytometry revealed that T cells constituted about 30% of CD45$^+$ cells isolated from tumors after vehicle or sunitinib, but accounted for 57% after mpJX-594 and 77% after mpJX-594 plus sunitinib (Fig. 5C). CD8$^+$ T cells predominated

Published OnlineFirst December 19, 2017; DOI: 10.1158/0008-5472.CAN-15-3308

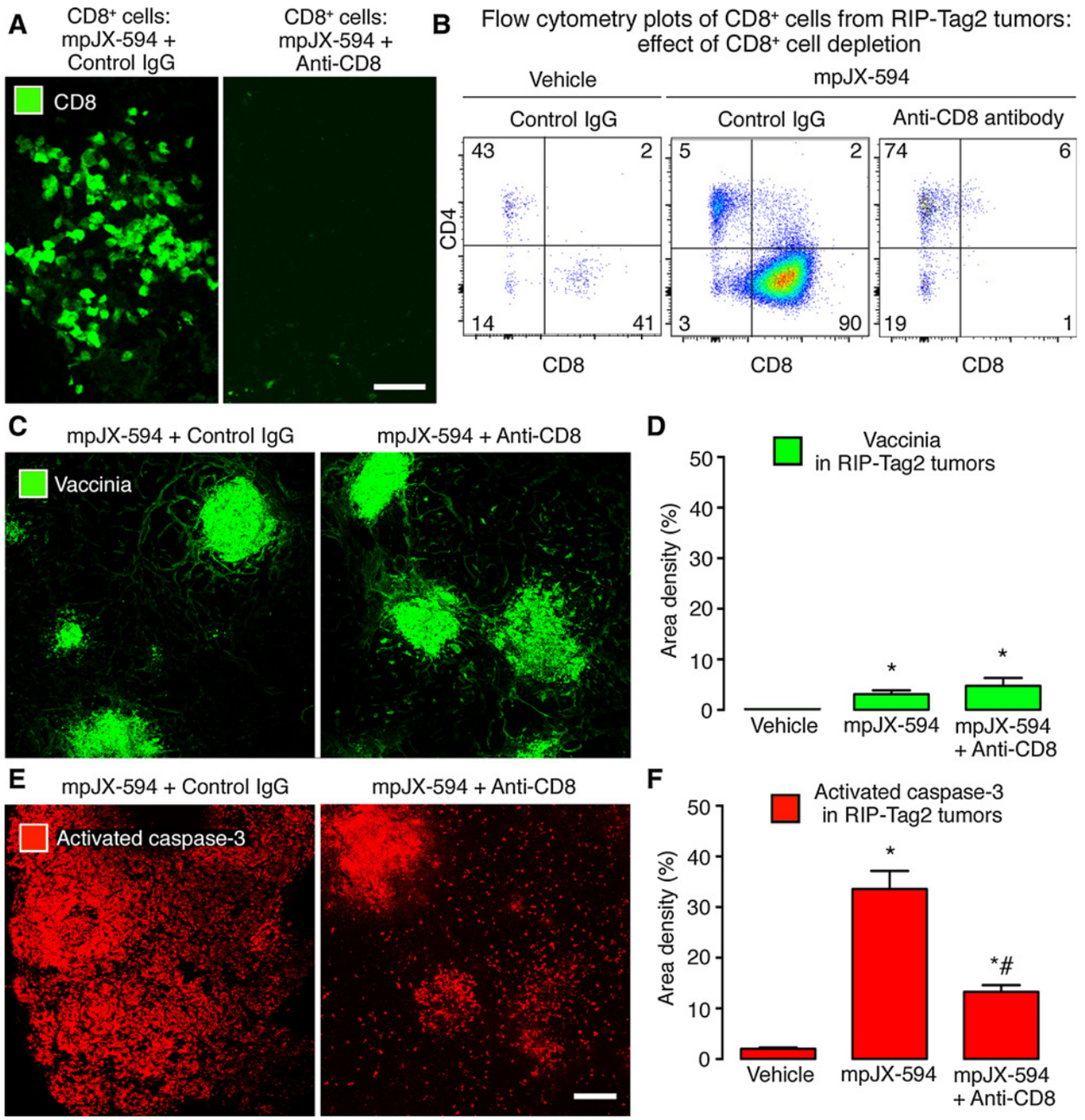

Figure 3.

Effects of CD8$^+$ T-cell depletion on vaccinia and apoptosis after mpJX-594. **A,** Confocal micrographs of CD8$^+$ T cells in RIP-Tag2 tumors at 5 days after mpJX-594 in mice with intact CD8$^+$ T cells (left) or after CD8$^+$ T-cell depletion (right) by anti-CD8 antibody. **B,** Flow cytometry plots of T cells (pregated on CD45$^+$/CD3$^+$) compared the small CD8$^+$ T-cell population after vehicle (left plot) with the large population at 5 days after mpJX-594 (center plot). CD8$^+$ T cells were not detected after mpJX-594 accompanied by CD8$^+$ T-cell depletion (right plot). **C,** Confocal micrographs of vaccinia staining in RIP-Tag2 tumor sections after mpJX-594 given with control IgG or anti-CD8 antibody as in **B**. **D,** Amounts of vaccinia staining after mpJX-594 were similar with or without CD8$^+$ T-cell depletion. Vaccinia was absent in vehicle-treated controls. **E,** Confocal micrographs of activated caspase-3 staining in tumor sections adjacent to those stained for vaccinia. Apoptotic cells in RIP-Tag2 tumors after mpJX-594 with anti-CD8$^+$ antibody are less abundant than with control IgG and are concentrated in regions of vaccinia staining. **F,** Greater activated caspase-3 staining after mpJX-594 but significantly less when virus was accompanied by CD8$^+$ T-cell depletion. ANOVA: $P < 0.05$ compared with vehicle (*) or with mpJX-594 plus control IgG ($n = 3$–6 mice/group; #). Scale bars, 50 μm in **A** and 200 μm in **E**.

in tumors after mpJX-594, averaging 13 times the number of CD4$^+$ T cells (Fig. 5D). CD8$^+$ to CD4$^+$ T-cell ratios were similar after mpJX-594 alone or with sunitinib, indicating similar enrichment of CD4$^+$ T cells and CD8$^+$ T cells (Fig. 5D). Tregs were less numerous after sunitinib given alone or with mpJX-594 than after mpJX-594 alone (Fig. 5E). More than 80% of CD8$^+$

Published OnlineFirst December 19, 2017; DOI: 10.1158/0008-5472.CAN-15-3308

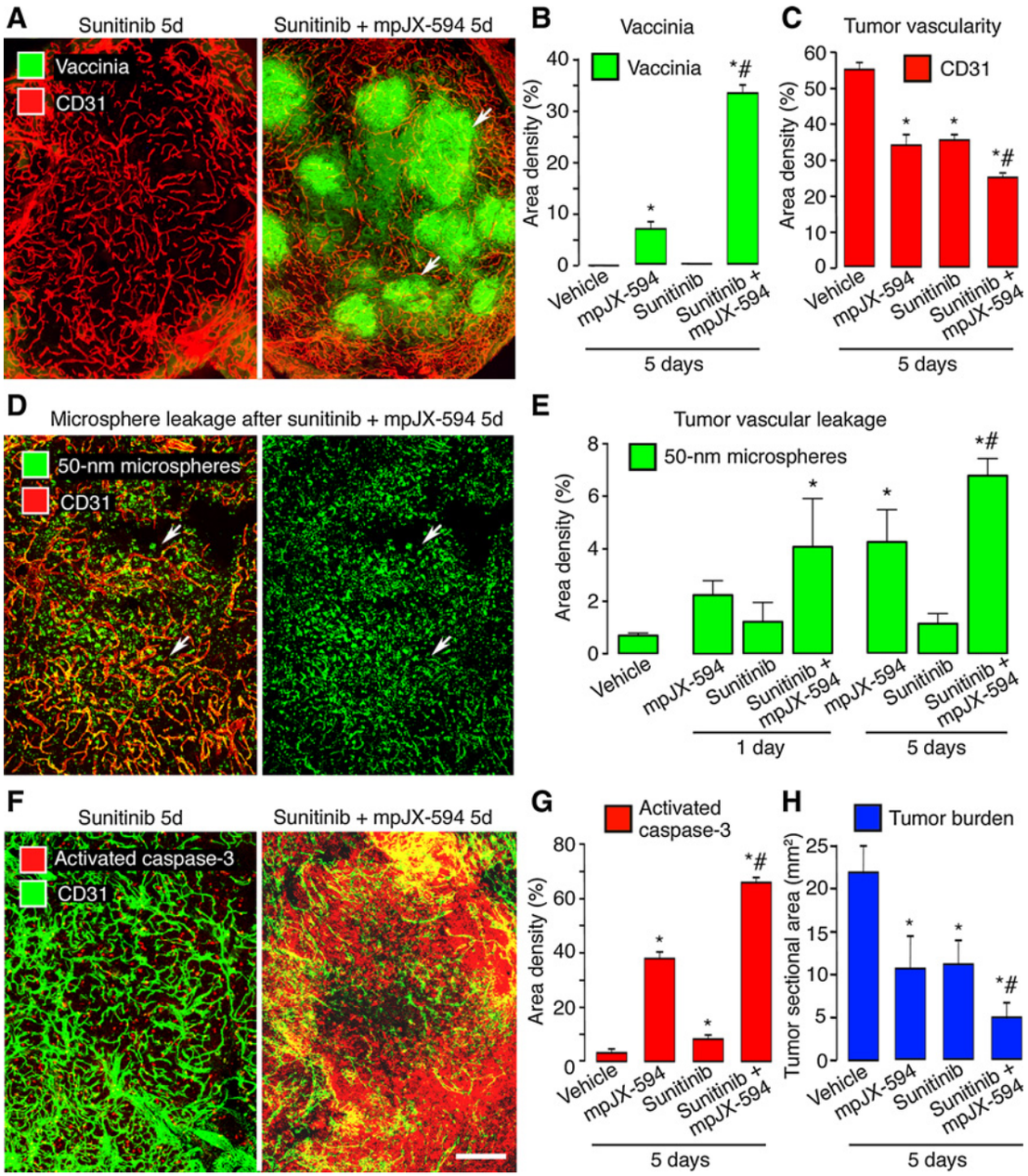

Figure 4.

Sunitinib amplification of mpJX-594 effects on tumor vascularity, leakage, and apoptosis. **A,** Confocal micrographs of blood vessels (CD31, red) and vaccinia (green, arrows) in RIP-Tag2 tumors at 5 days after daily sunitinib or one dose of mpJX-594 plus daily sunitinib. **B** and **C,** Treatment-related differences in vaccinia (**B**) and blood vessels (**C**) in tumors. ANOVA: $P < 0.05$ compared with vehicle (*) or with mpJX-594 alone ($n = 5$ mice/group; #). **D,** Widespread extravasation of 50-nm microspheres (green, arrows) in tumors at 5 days after mpJX-594 plus sunitinib. Intravascular microspheres removed by vascular perfusion 10 minutes after i.v. injection of tracer. Blood vessels, CD31, red. **E,** Extravasated microspheres were more abundant at 5 days after mpJX-594 than vehicle and were more numerous after mpJX-594 plus sunitinib than mpJX-594 alone. $P < 0.05$ compared with vehicle (*) or with mpJX-594 alone ($n = 4$ mice/group; #). **F,** Confocal micrographs show more apoptotic cells (activated caspase-3, red) in RIP-Tag2 tumor at 5 days after mpJX-594 plus sunitinib than sunitinib alone. Blood vessels (CD31, green). **G** and **H,** Treatment-related differences in activated caspase-3 (**G**) and tumor burden in pancreas (**H**). $P < 0.05$ compared with vehicle (*) or with mpJX-594 alone ($n = 5$ mice/group; #). Scale bar in **F** applies to all images, 200 μm.

T-cells were granzyme B^+ in tumors treated with mpJX-594 alone or with sunitinib, but few $CD8^+$/granzyme B^+ cells were found in the controls (Fig. 5F and G).

mpJX-594 plus sunitinib: Effects of treatment over 30 days

To determine whether the antitumor effects of the combination of agents were sustained during prolonged treatment, we gave two

Published OnlineFirst December 19, 2017; DOI: 10.1158/0008-5472.CAN-15-3308

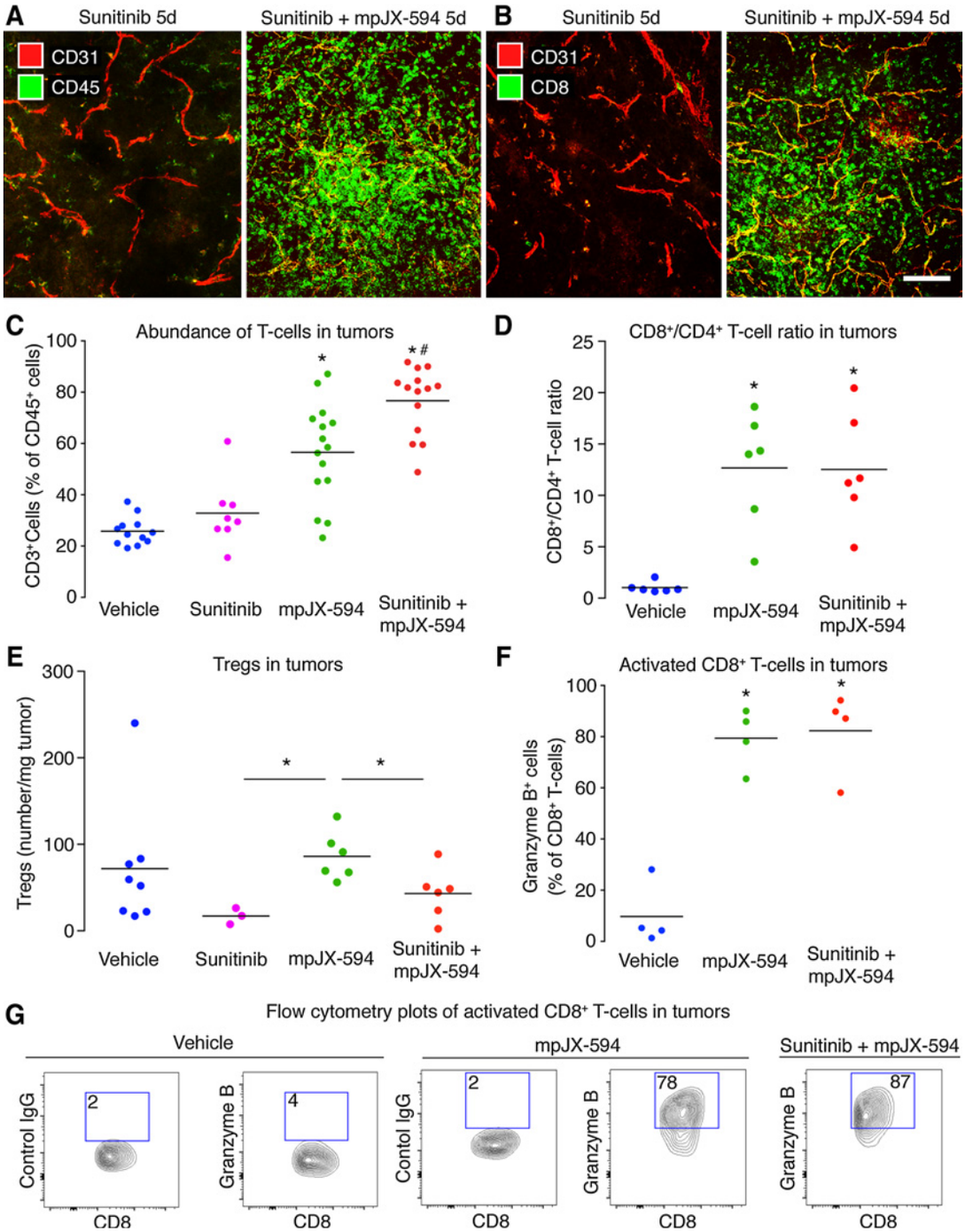

Figure 5.

CD8$^+$ T-cell influx after mpJX-594 plus sunitinib. **A** and **B,** Confocal micrographs of leukocytes stained for CD45 (green; **A**) or CD8 (green; **B**) and blood vessels (CD31, red) in RIP-Tag2 tumors at 5 days after sunitinib alone or with mpJX-594. **C,** Treatment-related differences in proportions of CD3$^+$ cells in CD45$^+$ leukocyte population assessed by flow cytometry. Each dot represents value for all tumors from one RIP-Tag2 mouse. ANOVA: $P < 0.05$ compared with vehicle (*) or with mpJX-594 alone ($n = 8$–15 mice/group; #). **D,** Ratio of CD8$^+$ T cells to CD4$^+$ T cells in tumors from mice at 5 days after vehicle, mpJX-594, or mpJX-594 plus sunitinib. ANOVA: *, $P < 0.05$ compared with vehicle ($n = 6$ mice/group). **E,** Treatment-related differences in Tregs (CD45$^+$/CD3$^+$/CD4$^+$/Foxp3$^+$) per mg tumor tissue at 5 days. No significant difference among groups by ANOVA, but *, $P < 0.05$ for differences between sunitinib or sunitinib plus mpJX-594 versus mpJX-594 alone by Student t tests ($n = 3$–8 mice/group). **F,** Treatment-related differences in CD8$^+$ T-cell activation shown by flow cytometry for granzyme B$^+$ staining. ANOVA: *, $P < 0.05$ compared with vehicle ($n = 4$ mice/group). **G,** Flow cytometry plots show gating and upregulation of granzyme B in CD8$^+$ T cells at 5 days after mpJX-594 alone or with sunitinib (% granzyme B$^+$ cells in boxes, pregated on CD45$^+$/CD3$^+$/CD8$^+$). Control antibody is mouse IgG of same isotype. Scale bar, 100 μm in **B**.

Published OnlineFirst December 19, 2017; DOI: 10.1158/0008-5472.CAN-15-3308

sequential doses of mpJX-594 with daily doses of sunitinib over 30 days. RIP-Tag2 mice were treated with mpJX-594 on days 0 and 15 and with sunitinib daily on days 5 to 29 (Fig. 6A). Other groups received a similar regimen of vehicle, mpJX-594 alone, or sunitinib alone (Fig. 6A). Compared with vehicle, all three treatments resulted in significant reduction in tumor vascularity, increase in apoptosis, and reduction in tumor burden (Fig. 6B–G). The amount of vascular pruning was about the same with all three treatments (Fig. 6B and C). However, compared with the single agents, the combination produced triple the amount of apoptosis (Fig. 6D and E) and more than twice the reduction in tumor burden (Fig. 6F and G).

mpJX-594 plus sunitinib: Effects on invasion and metastasis

Studies of RIP-Tag2 mice at 17 weeks of age made it possible to test the effects of mpJX-594 and sunitinib on tumor invasion and metastasis, which are common at this age (28, 40). Using the 30-day regimen (Fig. 6A), we examined the efficacy of mpJX-594 and sunitinib, given separately or together. Tumors treated with mpJX-594 alone had more distinct margins and less invasion, reflected by fewer tumor cells around pancreatic acinar cells, but tumors treated with the combination were even less invasive (Fig. 7A and B).

Microscopic liver metastases, detected by SV40 T-antigen staining (28, 41), were found in 100% of RIP-Tag2 mice treated with vehicle, mpJX-594, or sunitinib alone over the 30-day regimen, but were found in only 50% of mice treated with mpJX-594 plus sunitinib (Fig. 7C). The latter mice had 94% fewer micrometastases than vehicle-treated controls (Fig. 7D). Strong vaccinia staining was found in micrometastases but not elsewhere in the liver of 17-week-old mice given mpJX-594 5 days earlier (Fig. 7E). Most cells within micrometastases also stained for activated caspase-3 (Fig. 7E).

mpJX-594 plus sunitinib: Effects of administration sequence

Because sunitinib is reported to amplify the antitumor action of vaccinia virus only when given after the virus (19), we compared three sequences of administration to RIP-Tag2 mice (Supplementary Fig. S8A): (a) Simultaneous: mpJX-594 on day 0, and sunitinib daily on days 0–9; (b) mpJX-594 first: mpJX-594 on day 0, and sunitinib daily on days 5–9; and (c) Sunitinib first: sunitinib daily on days 0–9, and mpJX-594 on day 5. For comparison, mpJX-594 or sunitinib was given alone and studied at 5 and 10 days. Readouts were vaccinia staining, vascular density, and activated caspase-3. Values for mpJX-594 plus sunitinib on day 10 (Supplementary Fig. S8B–S8D) were normalized to the corresponding value for mpJX-594 alone (Supplementary Fig. S8E–S8G).

Vaccinia was significantly greater in the Simultaneous and mpJX-594 first groups than in the Sunitinib first group (Supplementary Fig. S8B). Tumor vascularity was reduced more in the Simultaneous and Sunitinib first groups than in the mpJX-594 first group (Supplementary Fig. S8C), as expected for sunitinib for 10 days versus 5 days. As an index of apoptosis in tumors, activated caspase-3 was greater in the Simultaneous and mpJX-594 first groups than in the Sunitinib first group (Supplementary Fig. S8D).

Vaccinia staining was greater at 5 days than at 10 days after mpJX-594 alone (Supplementary Fig. S8E). Tumor vascularity was reduced about the same amount by mpJX-594 alone as by sunitinib alone, and the reduction was greater at 10 days than 5 days (Supplementary Fig. S8F). Activated caspase-3 was more widespread after mpJX-594 than after sunitinib at 5 or 10 days (Supplementary Fig. S8G). Tumor burden was similarly decreased by mpJX-594 plus sunitinib regardless of the administration sequence (Supplementary Fig. S8H).

mpJX-594 plus sunitinib: Effects not mimicked by VEGFR2 inhibition by DC101

To determine whether sunitinib amplification of the antitumor effects of mpJX-594 resulted from the antiangiogenic effects of blocking VEGF signaling, we used the selective VEGFR2 inhibitor DC101 in place of sunitinib (Supplementary Fig. S9A). The large increase in vaccinia staining found when mpJX-594 was combined with sunitinib was not found when the virus was combined with DC101 (Supplementary Fig. S9B and S9C). Vaccinia staining was similar regardless of whether mpJX-594 was given alone or with two (2×) or three doses (3×) of DC101 (Supplementary Fig. S9B and S9C). The reduction in tumor vascularity after DC101 was about the same as after sunitinib, but was greater after sunitinib plus mpJX-594 than the other treatments (Supplementary Fig. S9D). Treatment-related differences in activated caspase-3 in RIP-Tag2 tumors (Supplementary Fig. S9E) correlated with, but was consistently greater than, the amount of vaccinia staining (Supplementary Fig. S9F).

Discussion

This study sought to identify factors that regulate tumor cell killing in spontaneous pancreatic neuroendocrine tumors after i.v. injection of oncolytic vaccinia virus mpJX-594 into RIP-Tag2 mice. Experiments revealed that the virus initially infected tumor blood vessels, but not normal blood vessels, and subsequently spread to focal regions of tumor cells that underwent oncolysis. However, tumor cell killing was much more widespread than the infection. Widespread tumor cell killing at 5 days was dependent on $CD8^+$ T cells, as shown by $CD8^+$ T-cell depletion, but was not dependent on viral GM-CSF, as reflected by equivalent tumor cell killing by mpJX-594 variants that expressed human GM-CSF, mouse GM-CSF, or no GM-CSF. Coadministration of sunitinib with mpJX-594 amplified vascular pruning and leakage in tumors, reduction of tumor burden, and suppression of invasion and metastasis. These effects were not mimicked by selective inhibition of VEGFR2 by DC101 antibody but were accompanied by reduction in Tregs and greater influx of activated $CD8^+$ T-cells.

mpJX-594 effects on RIP-Tag2 tumors and U87 gliomas

Oncolytic vaccinia viruses are reported to infect the vasculature of tumors and promote vascular collapse and necrosis (16–19). Infection of tumor vasculature has been described in biopsies from patients 7 days after a single i.v. infusion of JX-594 (18). Our findings of widespread extravasation of fibrin, erythrocytes, and 50-nm microspheres in RIP-Tag2 tumors 5 days after mpJX-594 confirm the disruption of the endothelial barrier but argue against vascular collapse because leakage of these blood-borne tracers required blood flow.

RIP-Tag2 transgenic mice were used to study effects of oncolytic vaccinia viral infection on tumors that develop in their natural microenvironment and progress through the stages observed in humans (26–28). Time-course experiments revealed that vaccinia virus initially infected and replicated in endothelial cells of tumor vessels, where vaccinia and YFP staining were visible at 6 hours and longer after i.v. injection of mpJX-594. Extravasation

Published OnlineFirst December 19, 2017; DOI: 10.1158/0008-5472.CAN-15-3308

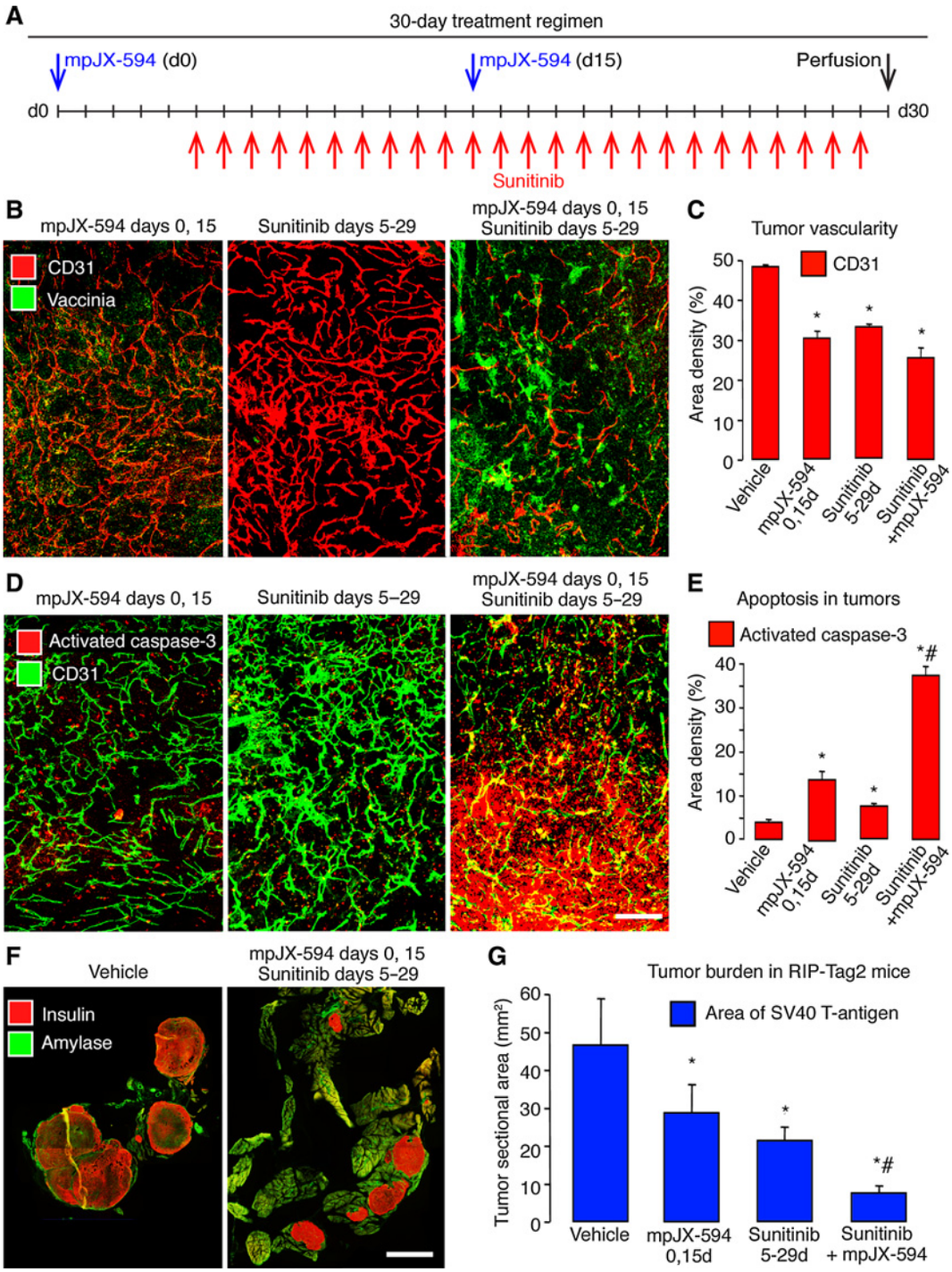

Figure 6.

mpJX-594 plus sunitinib: 30-day treatment of RIP-Tag2 mice. **A,** Treatment regimens for mpJX-594 (2 doses, days 0, 15) and sunitinib (25 doses, days 5–29) individually or together. Controls received vehicle for 30 days. **B,** Confocal micrographs show treatment-related differences in vaccinia (green) and blood vessels (CD31, red) in tumors. **C,** Treatment-related differences in tumor vascularity. **D,** Confocal micrographs compare abundance of apoptotic cells (activated caspase-3, red) and blood vessels (CD31, green) after three treatments. **E,** Treatment-related differences activated caspase-3 in tumors. **F,** Tumor cells (insulin, red) and pancreatic acinar cells (amylase, green) after treatment with vehicle (left) or mpJX-594 plus sunitinib over 30 days (right). **G,** Treatment-related differences in tumor burden assessed as total sectional area of SV40 T-antigen–stained tumors in the pancreas. ANOVA for comparisons in **C**, **E**, and **G**. $P < 0.05$ compared with vehicle (*) or with mpJX-594 alone or sunitinib alone ($n = 5$ mice/group; #). Scale bar in **F** applies to all images, 200 μm in **B** and **D**, and 3 mm in **F**.

Published OnlineFirst December 19, 2017; DOI: 10.1158/0008-5472.CAN-15-3308

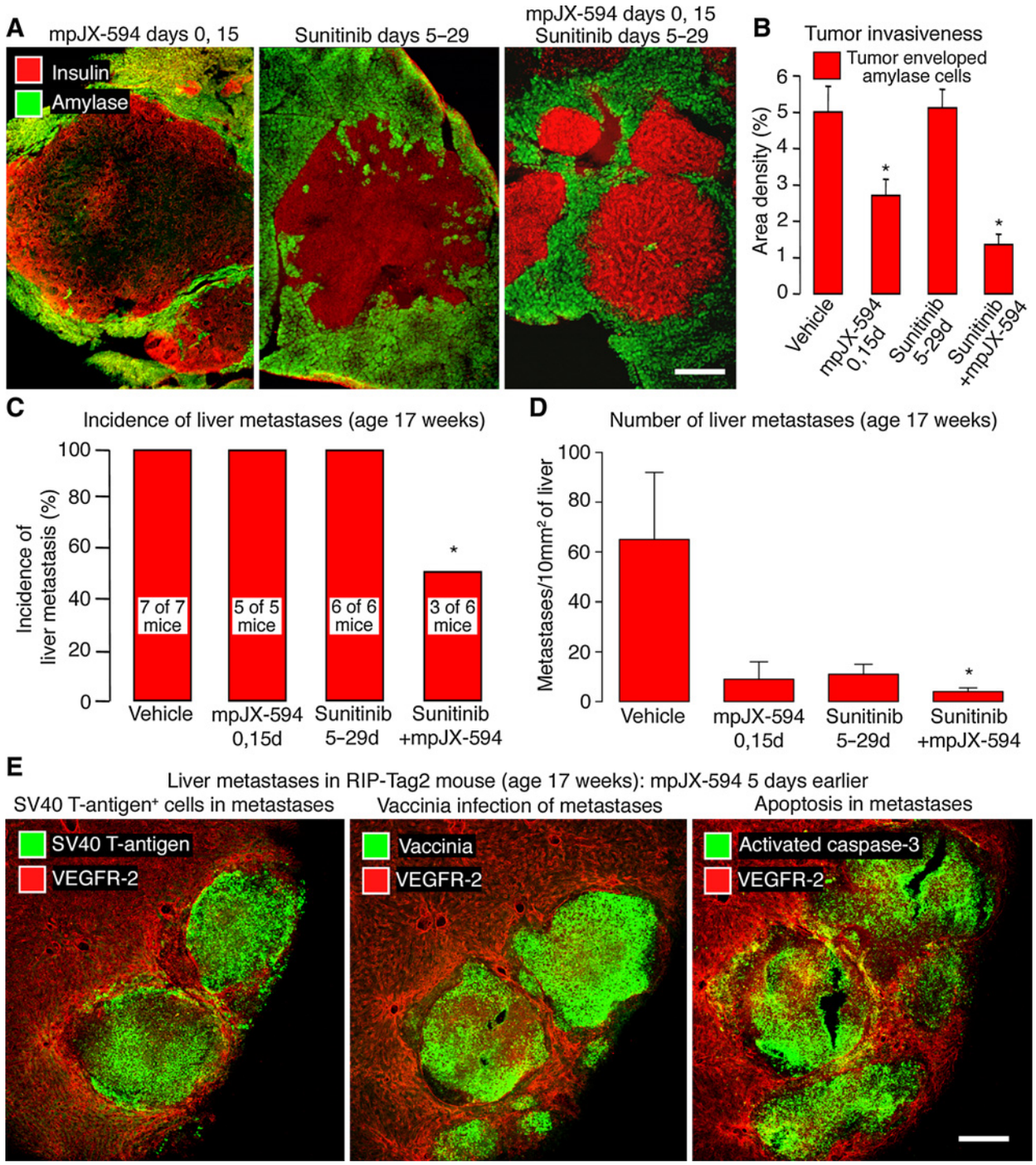

Figure 7.

mpJX-594 plus sunitinib: Effects on invasion and metastasis. **A,** Confocal micrographs show treatment-related differences in invasion of tumor cells (insulin, red) into acinar pancreas (amylase, green) of RIP-Tag2 mice (treatment regimens in **A**). Tumor treated with sunitinib for 25 days is the most invasive, reflected by highly irregular border contour. **B,** Treatment-related differences in amount of invasion indicated by tumor cells surrounding acinar cells. ANOVA: *, $P < 0.05$ compared with vehicle ($n = 5$ mice/group). **C,** Treatment-related differences in incidence of liver micrometastases. Number of mice with metastases shown on bars. Fisher exact test: *, $P = 0.0247$. **D,** Treatment-related differences in abundance of liver micrometastases expressed per 10 mm^2 of section area. ANOVA: *, $P < 0.05$ compared with vehicle ($n = 5$ mice/group). **E,** Confocal micrographs of liver of 17-week-old mouse 5 days after i.v. injection of mpJX-594. Sequential sections stained for blood vessels (VEGFR2, red) and tumor cells (SV40 T-antigen, green, left), vaccinia (green, center), or apoptotic cells (activated caspase-3, green, right). Scale bar in **E** applies to all images, 300 μm for **A** and 200 μm for **E**.

Published OnlineFirst December 19, 2017; DOI: 10.1158/0008-5472.CAN-15-3308

increased from 1 to 5 days. Parallel changes were found in U87 gliomas. These findings fit with a sequence where viral infection of endothelial cells led to disrupted barrier function and subsequent infection of tumor cells.

Contribution of CD8$^+$ T-cell influx to mpJX-594 tumor cell killing

Apoptosis was widespread in tumors 5 days after mpJX-594, similar to other oncolytic viruses (42). After mpJX-594, activated caspase-3 in tumors was much more widespread than vaccinia infection. The difference was more than 5-fold at 5 days.

Activated CD8$^+$ T cells were greatly increased in tumors of RIP-Tag2 mice treated with mpJX-594. Similarly, T-cell infiltration and widespread necrosis have been found in tumors of humans treated with JX-594/Pexa-Vec (10, 12).

The contribution of the immune response to the large amount of tumor cell apoptosis was examined by depleting CD8$^+$ T cells by prior administration of anti-CD8 antibody. In the absence of CD8$^+$ T cells, tumor cell killing at 5 days after mpJX-594 was limited to focal regions of vaccinia infection. The magnitude of infection was not reduced. These observations fit with the finding that intratumoral administration of oncolytic virus not only affects injected tumors but also affects noninjected metastases (5), and with other evidence for bystander effects due to virally triggered tumor-specific immunity (43).

Contribution of GM-CSF expression to mpJX-594 tumor cell killing

mpJX-594, like its clinical counterpart JX-594/Pexa-Vec, expresses human GM-CSF (18, 29). Because of the limited activity of human GM-CSF in mice (30, 31), we tested the contribution of GM-CSF by comparing variants of mpJX-594 that express human GM-CSF, mouse GM-CSF, or no GM-CSF. We sought to learn whether GM-CSF contributed to the CD8$^+$ T-cell–dependent, widespread tumor cell killing evident at 5 days. Although GM-CSF dependency seemed unlikely, because more than 5 days should be needed for maximal viral GM-CSF production and effect, we considered it important to determine whether mpJX-594 could induce widespread tumor cell killing in the absence of GM-CSF. The finding of widespread apoptosis in tumors at 5 days in strikingly similar amounts after all three variants of mpJX-594 indicates that viral GM-CSF made little or no contribution to tumor cell killing under these conditions. More prolonged studies with the three mpJX-594 variants would be needed to determine the contribution of viral GM-CSF at later time points. Indeed, greater efficacy of vaccinia virus that expresses GM-CSF has been reported in rabbits treated for 10 weeks (44).

Sunitinib amplification of mpJX-594 effects on tumors

Oncolytic vaccinia viral infection of endothelial cells can reduce tumor blood flow in mouse models (16) and cancer patients (18), but perfusion recovers as vaccinia virus is cleared (19). Sunitinib and other inhibitors of VEGF signaling are thought to increase efficacy and persistence of vaccinia viral effects by inhibiting angiogenesis and revascularization in tumors (19).

Sunitinib amplified mpJX-594 infection, vascular pruning, leakage, CD8$^+$ T-cell recruitment, and apoptosis in tumors, and reduced invasion and metastasis in RIP-Tag2 mice. In dissecting the complementary effects of mpJX-594 and sunitinib, we considered the effects each had on the tumor vasculature. Sunitinib and other angiogenesis inhibitors are known to prune tumor blood vessels and leave behind "normalized" vessels (28, 36, 45). However, reduction in tumor vascularity is an unlikely explanation for sunitinib amplification of mpJX-594, because sunitinib alone caused as much vascular pruning but had little effect on tumor cell killing. Even with the 30-day treatment regimen, the amount of apoptosis after mpJX-594 plus sunitinib was almost 3-fold greater than after mpJX-594 alone, but tumor vascularity was about the same.

After administration of mpJX-594 alone or with sunitinib, tumor vessels had sustained blood flow but were more leaky, instead of the normalization typical of sunitinib (28, 45). Leakiness continued for at least 5 days. Tumor vascular leakiness is reported to improve oncolytic viral delivery and efficacy in some tumor models (21, 46). Sunitinib given briefly before reovirus is thought to increase efficacy by causing a rebound burst of VEGF signaling in tumor endothelial cells, which promotes viral replication, cell lysis, leakage, and immune-mediated effects followed by vascular collapse (21). Vascular collapse did not occur in RIP-Tag2 tumors after mpJX-594, as reflected by sustained blood flow and extravasation of microspheres, and was thus an unlikely cause of the amplified antitumor actions.

Tregs were present in RIP-Tag2 tumors in numbers reported for other tumor models (13, 47). Sunitinib increases CD8$^+$ T-cell recruitment and promotes an immunogenic tumor microenvironment by suppressing Tregs and MDSCs (22–24). Our finding of significantly fewer Tregs and more abundant activated CD8$^+$ T cells in RIP-Tag2 tumors after mpJX-594 plus sunitinib than after mpJX-594 alone is consistent with these reports. Because CD4$^+$ T cells and CD8$^+$ T cells were similarly enriched after mpJX-594, cytotoxic CD4$^+$ T cells could also contribute to antitumor immunity (48). Oncolytic viruses can also promote innate immunity and immune-cell infiltration of tumors by releasing cytokines and other factors from lysed tumor cells (49–51).

Influence of sequence of administration

To determine the influence of administration sequence, we treated RIP-Tag2 mice with mpJX-594 plus sunitinib together (Simultaneous) or 5 days apart (mpJX-594 first or Sunitinib first). Simultaneous and mpJX-594 first were more effective than Sunitinib first in increasing apoptosis in tumors, but all regimens were similarly effective in reducing tumor burden at 10 days. In contrast, DC101 given before or after mpJX-594 tended to decrease vaccinia infection, consistent with evidence for VEGF influence on oncolytic viral infection in endothelial cells (17, 19–21).

Instead of simply blocking VEGF signaling and angiogenesis, sunitinib amplification of mpJX-594 effects fits better with a mechanism whereby sunitinib suppressed viral resistance, augmented mpJX-594 infection, reduced Tregs, and amplified activated CD8$^+$ T-cell in tumors. As a precedent, sunitinib increases oncolytic VSV infection by suppressing host genes (24, 25, 52). These actions would reconcile the difference between the effects of sunitinib and selective VEGFR2 blockade by DC101.

mpJX-594 effects on metastasis

Importantly, after i.v. administration mpJX-594 not only reduced the size of primary tumors but also infected and induced apoptosis in liver metastases in RIP-Tag2 mice, which to our knowledge has not been reported previously. mpJX-594 given

Published OnlineFirst December 19, 2017; DOI: 10.1158/0008-5472.CAN-15-3308

with sunitinib reduced invasion and the incidence, number, and size of liver micrometastases in RIP-Tag2 mice treated until 17 weeks of age, when liver metastases are common (28, 40). These findings indicate that sunitinib given with mpJX-594 did not have the proinvasive and prometastatic properties reported for sunitinib given alone to RIP-Tag2 mice (28). The amplified level of vaccinia infection and $CD8^+$ T-cell influx in tumors could contribute to the greater reduction in tumor burden. The lack of significant survival benefit in the 30-day experiment probably resulted from the dominance of hypoglycemia and other metabolic changes over tumor burden in governing longevity of RIP-Tag2 mice (28).

Translational relevance

JX-594/Pexa-Vec administered intratumorally or intravenously has undergone phase I and II testing alone and in combination with other therapies for cancer in adults (8, 10, 11, 53, 54) and phase I testing in pediatric cancer patients (29). Treatment of hepatocellular carcinoma by JX-594 plus sorafenib was accompanied by significant reduction of tumor vascular perfusion, sustained tumor necrosis, and prolongation of survival (17). In this trial, JX-594 was given first because sorafenib, as a Raf kinase inhibitor, affects JX-594 replication, which is promoted by EGFR/Ras pathway activation in cancer cells (55). In the same trial, 1 patient with renal cell carcinoma, who received sunitinib after participating in a JX-594 dose-escalation trial, had a whole-body tumor response (17). Randomized clinical trials will determine whether JX-594 followed by sunitinib is more efficacious than either agent alone in cancer patients.

In conclusion, oncolytic vaccinia virus mpJX-594 given by i.v. injection rapidly infects tumor vascular endothelial cells and results in sustained leakage, spread of virus to tumor cells, influx of $CD8^+$ T cells, and widespread tumor cell killing. In the absence of $CD8^+$ T cells, tumor cell killing is largely restricted to infected regions of tumors. Viral GM-CSF does not contribute to the $CD8^+$ T-cell–dependent, widespread tumor cell killing by mpJX-594 evident at 5 days. Coadministration of sunitinib amplifies the antitumor effects on primary tumors and metastases, mainly by augmenting the viral infection, reducing Tregs, and increasing activated $CD8^+$ T cells, rather than inhibiting angiogenesis. Together, the findings support the rationale for combining oncolytic vaccinia viruses with sunitinib in the treatment of cancer patients.

Disclosure of Potential Conflicts of Interest

J.C. Bell is among the Board of Directors of, has ownership interest (including patents) in, and is a consultant/advisory board member for Turnstone Biologics. D.H. Kirn has employment, compensation and ownership interest in the form of stock in Ignite Immunotherapy and in 4D Molecular Therapeutics. N. De Silva has ownership interest (including patents) in SillaJen Biotherapeutics, Inc. C.J. Breitbach has ownership interest (including patents) in and is a consultant/advisory board member for SillaJen. No potential conflicts of interest were disclosed by the other authors.

Authors' Contributions

Conception and design: M. Kim, M. Nitschké, B. Sennino, B.J. Schriver, D.H. Kirn, J.C. Bell, N. De Silva, C.J. Breitbach, D.M. McDonald

Development of methodology: M. Nitschké, B. Sennino, B.J. Schriver, C.E. McDonald, J. Wang, D.H. Kirn, N. De Silva, C.J. Breitbach, D.M. McDonald

Acquisition of data (provided animals, acquired and managed patients, provided facilities, etc.): M. Kim, M. Nitschké, B. Sennino, P. Murer, B.J. Schriver, A. Bell, A. Subramanian, C.E. McDonald, H. Cha, M.-C. Bourgeois-Daigneault, N. De Silva, D.M. McDonald

Analysis and interpretation of data (e.g., statistical analysis, biostatistics, computational analysis): M. Kim, M. Nitschké, B. Sennino, P. Murer, B.J. Schriver, A. Bell, A. Subramanian, C.E. McDonald, D.H. Kirn, N. De Silva, C.J. Breitbach, D.M. McDonald

Writing, review, and/or revision of the manuscript: M. Kim, M. Nitschké, B. Sennino, P. Murer, B.J. Schriver, A. Bell, J. Wang, D.H. Kirn, J.C. Bell, N. De Silva, C.J. Breitbach, D.M. McDonald

Administrative, technical, or material support (i.e., reporting or organizing data, constructing databases): M. Kim, M. Nitschké, P. Murer, C.J. Breitbach, D.M. McDonald

Study supervision: M. Nitschké, P. Murer, C.J. Breitbach, D.M. McDonald

Acknowledgments

This work was supported in part by funding from SillaJen Biotherapeutics and grants to DMcD from the National Heart, Lung, and Blood Institute (R01 HL059157, R01 HL127402, and P01 HL024136) of the US National Institutes of Health, and funding from the Leducq Foundation Transatlantic Network of Excellence (grant 11CVD03) and from Angel-Works Foundation.

The costs of publication of this article were defrayed in part by the payment of page charges. This article must therefore be hereby marked *advertisement* in accordance with 18 U.S.C. Section 1734 solely to indicate this fact.

Received December 9, 2015; revised October 30, 2017; accepted December 15, 2017; published OnlineFirst December 19, 2017.

References

1. Zeh HJ, Downs-Canner S, McCart JA, Guo ZS, Rao UN, Ramalingam L, et al. First-in-man study of western reserve strain oncolytic vaccinia virus: safety, systemic spread, and antitumor activity. Mol Ther 2015;23:202–14.
2. Puzanov I, Milhem MM, Minor D, Hamid O, Li A, Chen L, et al. Talimogene laherparepvec in combination with ipilimumab in previously untreated, unresectable stage IIIB-IV melanoma. J Clin Oncol 2016;34:2619–26.
3. Breitbach CJ, Lichty BD, Bell JC. Oncolytic viruses: therapeutics with an identity crisis. EBioMedicine 2016;9:31–6.
4. Lawler SE, Speranza MC, Cho CF, Chiocca EA. Oncolytic viruses in cancer treatment: a review. JAMA Oncol 2017;3:841–49.
5. Ribas A, Dummer R, Puzanov I, VanderWalde A, Andtbacka RHI, Michielin O, et al. Oncolytic virotherapy promotes intratumoral T cell infiltration and improves anti-PD-1 immunotherapy. Cell 2017;170:1109–19e10.
6. Kim JH, Oh JY, Park BH, Lee DE, Kim JS, Park HE, et al. Systemic armed oncolytic and immunologic therapy for cancer with JX-594, a targeted poxvirus expressing GM-CSF. Mol Ther 2006;14:361–70.
7. Merrick AE, Ilett EJ, Melcher AA. JX-594, a targeted oncolytic poxvirus for the treatment of cancer. Curr Opin Investig Drugs 2009;10:1372–82.
8. Park SH, Breitbach CJ, Lee J, Park JO, Lim HY, Kang WK, et al. Phase 1b trial of biweekly intravenous Pexa-Vec (JX-594), an oncolytic and immunotherapeutic vaccinia virus in colorectal cancer. Mol Ther 2015;23:1532–40.
9. Breitbach CJ, Parato K, Burke J, Hwang TH, Bell JC, Kirn DH. Pexa-Vec double agent engineered vaccinia: oncolytic and active immunotherapeutic. Curr Opin Virol 2015;13:49–54.
10. Hwang TH, Moon A, Burke J, Ribas A, Stephenson J, Breitbach CJ, et al. A mechanistic proof-of-concept clinical trial with JX-594, a targeted multi-mechanistic oncolytic poxvirus, in patients with metastatic melanoma. Mol Ther 2011;19:1913–22.
11. Heo J, Reid T, Ruo L, Breitbach CJ, Rose S, Bloomston M, et al. Randomized dose-finding clinical trial of oncolytic immunotherapeutic vaccinia JX-594 in liver cancer. Nat Med 2013;19:329–36.
12. Kim MK, Breitbach CJ, Moon A, Heo J, Lee YK, Cho M, et al. Oncolytic and immunotherapeutic vaccinia induces antibody-mediated complement-

dependent cancer cell lysis in humans. Sci Transl Med 2013;5:185ra63.
13. Zamarin D, Holmgaard RB, Subudhi SK, Park JS, Mansour M, Palese P, et al. Localized oncolytic virotherapy overcomes systemic tumor resistance to immune checkpoint blockade immunotherapy. Sci Transl Med 2014;6:226ra32.
14. Lawson KA, Mostafa AA, Shi ZQ, Spurrell J, Chen W, Kawakami J, et al. Repurposing sunitinib with oncolytic reovirus as a novel immunotherapeutic strategy for renal cell carcinoma. Clin Cancer Res 2016;22:5839–50.
15. Hou W, Sampath P, Rojas JJ, Thorne SH. Oncolytic virus-mediated targeting of PGE2 in the tumor alters the immune status and sensitizes established and resistant tumors to immunotherapy. Cancer Cell 2016;30:108–19.
16. Breitbach CJ, De Silva NS, Falls TJ, Aladl U, Evgin L, Paterson J, et al. Targeting tumor vasculature with an oncolytic virus. Mol Ther 2011;19:886–94.
17. Heo J, Breitbach CJ, Moon A, Kim CW, Patt R, Kim MK, et al. Sequential therapy with JX-594, a targeted oncolytic poxvirus, followed by sorafenib in hepatocellular carcinoma: preclinical and clinical demonstration of combination efficacy. Mol Ther 2011;19:1170–9.
18. Breitbach CJ, Arulanandam R, De Silva N, Thorne SH, Patt R, Daneshmand M, et al. Oncolytic vaccinia virus disrupts tumor-associated vasculature in humans. Cancer Res 2013;73:1265–75.
19. Hou W, Chen H, Rojas J, Sampath P, Thorne SH. Oncolytic vaccinia virus demonstrates antiangiogenic effects mediated by targeting of VEGF. Int J Cancer 2014;135:1238–46.
20. Arulanandam R, Batenchuk C, Angarita FA, Ottolino-Perry K, Cousineau S, Mottashed A, et al. VEGF-mediated induction of PRD1-BF1/Blimp1 expression sensitizes tumor vasculature to oncolytic virus infection. Cancer Cell 2015;28:210–24.
21. Kottke T, Hall G, Pulido J, Diaz RM, Thompson J, Chong H, et al. Antiangiogenic cancer therapy combined with oncolytic virotherapy leads to regression of established tumors in mice. J Clin Invest 2010;120:1551–60.
22. Finke JH, Rini B, Ireland J, Rayman P, Richmond A, Golshayan A, et al. Sunitinib reverses type-1 immune suppression and decreases T-regulatory cells in renal cell carcinoma patients. Clin Cancer Res 2008;14:6674–82.
23. Terme M, Pernot S, Marcheteau E, Sandoval F, Benhamouda N, Colussi O, et al. VEGFA-VEGFR pathway blockade inhibits tumor-induced regulatory T-cell proliferation in colorectal cancer. Cancer Res 2013;73:539–49.
24. Draghiciu O, Nijman HW, Hoogeboom BN, Meijerhof T, Daemen T. Sunitinib depletes myeloid-derived suppressor cells and synergizes with a cancer vaccine to enhance antigen-specific immune responses and tumor eradication. Oncoimmunology 2015;4:e989764.
25. Jha BK, Dong B, Nguyen CT, Polyakova I, Silverman RH. Suppression of antiviral innate immunity by sunitinib enhances oncolytic virotherapy. Mol Ther 2013;21:1749–57.
26. Hanahan D. Heritable formation of pancreatic beta-cell tumours in transgenic mice expressing recombinant insulin/simian virus 40 oncogenes. Nature 1985;315:115–22.
27. Bergers G, Javaherian K, Lo KM, Folkman J, Hanahan D. Effects of angiogenesis inhibitors on multistage carcinogenesis in mice. Science 1999;284:808–12.
28. Sennino B, Ishiguro-Oonuma T, Wei Y, Naylor RM, Williamson CW, Bhagwandin V, et al. Suppression of tumor invasion and metastasis by concurrent inhibition of c-Met and VEGF signaling in pancreatic neuroendocrine tumors. Cancer Discov 2012;2:270–87.
29. Cripe TP, Ngo MC, Geller JI, Louis CU, Currier MA, Racadio JM, et al. Phase 1 study of intratumoral Pexa-Vec (JX-594), an oncolytic and immunotherapeutic vaccinia virus, in pediatric cancer patients. Mol Ther 2015;23:602–8.
30. Shanafelt AB, Johnson KE, Kastelein RA. Identification of critical amino acid residues in human and mouse granulocyte-macrophage colony-stimulating factor and their involvement in species specificity. J Biol Chem 1991;266:13804–10.
31. Murray HW, Cervia JS, Hariprashad J, Taylor AP, Stoeckle MY, Hockman H. Effect of granulocyte-macrophage colony-stimulating factor in experimental visceral leishmaniasis. J Clin Invest 1995;95:1183–92.
32. Christensen JG. A preclinical review of sunitinib, a multitargeted receptor tyrosine kinase inhibitor with anti-angiogenic and antitumour activities. Ann Oncol 2007;18Suppl 10:x3–10.
33. Prewett M, Huber J, Li Y, Santiago A, O'Connor W, King K, et al. Antivascular endothelial growth factor receptor (fetal liver kinase 1) monoclonal antibody inhibits tumor angiogenesis and growth of several mouse and human tumors. Cancer Res 1999;59:5209–18.
34. Kirn DH, Thorne SH. Targeted and armed oncolytic poxviruses: a novel multi-mechanistic therapeutic class for cancer. Nat Rev Cancer 2009;9:64–71.
35. Mastrangelo MJ, Maguire HC Jr, Eisenlohr LC, Laughlin CE, Monken CE, McCue PA, et al. Intratumoral recombinant GM-CSF-encoding virus as gene therapy in patients with cutaneous melanoma. Cancer Gene Ther 1999;6:409–22.
36. Inai T, Mancuso M, Hashizume H, Baffert F, Haskell A, Baluk P, et al. Inhibition of vascular endothelial growth factor (VEGF) signaling in cancer causes loss of endothelial fenestrations, regression of tumor vessels, and appearance of basement membrane ghosts. Am J Pathol 2004;165:35–52.
37. Nagy JA, Brown LF, Senger DR, Lanir N, Van de Water L, Dvorak AM, et al. Pathogenesis of tumor stroma generation: a critical role for leaky blood vessels and fibrin deposition. Biochim Biophys Acta 1989;948:305–26.
38. Hashizume H, Baluk P, Morikawa S, McLean JW, Thurston G, Roberge S, et al. Openings between defective endothelial cells explain tumor vessel leakiness. Am J Pathol 2000;156:1363–80.
39. Nakahara T, Norberg SM, Shalinsky DR, Hu-Lowe DD, McDonald DM. Effect of inhibition of vascular endothelial growth factor signaling on distribution of extravasated antibodies in tumors. Cancer Res 2006;66:1434–45.
40. Moen I, Gebre M, Alonso-Camino V, Chen D, Epstein D, McDonald DM. Anti-metastatic action of FAK inhibitor OXA-11 in combination with VEGFR-2 signaling blockade in pancreatic neuroendocrine tumors. Clin Exp Metastasis 2015;32:799–817.
41. Paez-Ribes M, Allen E, Hudock J, Takeda T, Okuyama H, Vinals F, et al. Antiangiogenic therapy elicits malignant progression of tumors to increased local invasion and distant metastasis. Cancer Cell 2009;15:220–31.
42. Cary ZD, Willingham MC, Lyles DS. Oncolytic vesicular stomatitis virus induces apoptosis in U87 glioblastoma cells by a type II death receptor mechanism and induces cell death and tumor clearance in vivo. J Virol 2011;85:5708–17.
43. Bartlett DL, Liu Z, Sathaiah M, Ravindranathan R, Guo Z, He Y, et al. Oncolytic viruses as therapeutic cancer vaccines. Mol Cancer 2013;12:103.
44. Lee JH, Roh MS, Lee YK, Kim MK, Han JY, Park BH, et al. Oncolytic and immunostimulatory efficacy of a targeted oncolytic poxvirus expressing human GM-CSF following intravenous administration in a rabbit tumor model. Cancer Gene Ther 2010;17:73–9.
45. Jain RK. Normalizing tumor microenvironment to treat cancer: bench to bedside to biomarkers. J Clin Oncol 2013;31:2205–18.
46. Tseng JC, Granot T, DiGiacomo V, Levin B, Meruelo D. Enhanced specific delivery and targeting of oncolytic Sindbis viral vectors by modulating vascular leakiness in tumor. Cancer Gene Ther 2010;17:244–55.
47. Jang JE, Hajdu CH, Liot C, Miller G, Dustin ML, Bar-Sagi D. Crosstalk between regulatory T cells and tumor-associated dendritic cells negates anti-tumor immunity in pancreatic cancer. Cell Rep 2017;20:558–71.
48. Akhmetzyanova I, Zelinskyy G, Littwitz-Salomon E, Malyshkina A, Dietze KK, Streeck H, et al. CD137 agonist therapy can reprogram regulatory T cells into cytotoxic CD4+ T cells with antitumor activity. J Immunol 2016;196:484–92.
49. Benencia F, Courreges MC, Conejo-Garcia JR, Mohamed-Hadley A, Zhang L, Buckanovich RJ, et al. HSV oncolytic therapy upregulates interferon-inducible chemokines and recruits immune effector cells in ovarian cancer. Mol Ther 2005;12:789–802.
50. Greiner S, Humrich JY, Thuman P, Sauter B, Schuler G, Jenne L. The highly attenuated vaccinia virus strain modified virus Ankara induces apoptosis in melanoma cells and allows bystander dendritic cells to generate a potent anti-tumoral immunity. Clin Exp Immunol 2006;146:344–53.
51. Endo Y, Sakai R, Ouchi M, Onimatsu H, Hioki M, Kagawa S, et al. Virus-mediated oncolysis induces danger signal and stimulates cytotoxic T-lymphocyte activity via proteasome activator upregulation. Oncogene 2008;27:2375–81.

Published OnlineFirst December 19, 2017; DOI: 10.1158/0008-5472.CAN-15-3308

52. Jha BK, Polyakova I, Kessler P, Dong B, Dickerman B, Sen GC, et al. Inhibition of RNase L and RNA-dependent protein kinase (PKR) by sunitinib impairs antiviral innate immunity. J Biol Chem 2011;286: 26319–26.
53. Park BH, Hwang T, Liu TC, Sze DY, Kim JS, Kwon HC, et al. Use of a targeted oncolytic poxvirus, JX-594, in patients with refractory primary or metastatic liver cancer: a phase I trial. Lancet Oncol 2008;9:533–42.
54. Breitbach CJ, Burke J, Jonker D, Stephenson J, Haas AR, Chow LQ, et al. Intravenous delivery of a multi-mechanistic cancer-targeted oncolytic poxvirus in humans. Nature 2011;477:99–102.
55. Parato KA, Breitbach CJ, Le Boeuf F, Wang J, Storbeck C, Ilkow C, et al. The oncolytic poxvirus JX-594 selectively replicates in and destroys cancer cells driven by genetic pathways commonly activated in cancers. Mol Ther 2012;20:749–58.

Cancer Research
The Journal of Cancer Research (1916–1930) | The American Journal of Cancer (1931–1940)

AACR American Association for Cancer Research

Amplification of Oncolytic Vaccinia Virus Widespread Tumor Cell Killing by Sunitinib through Multiple Mechanisms

Minah Kim, Maximilian Nitschké, Barbara Sennino, et al.

Cancer Res 2018;78:922-937. Published OnlineFirst December 19, 2017.

mpJX-594 vaccinia virus variants used to test contribution of GM-CSF expression

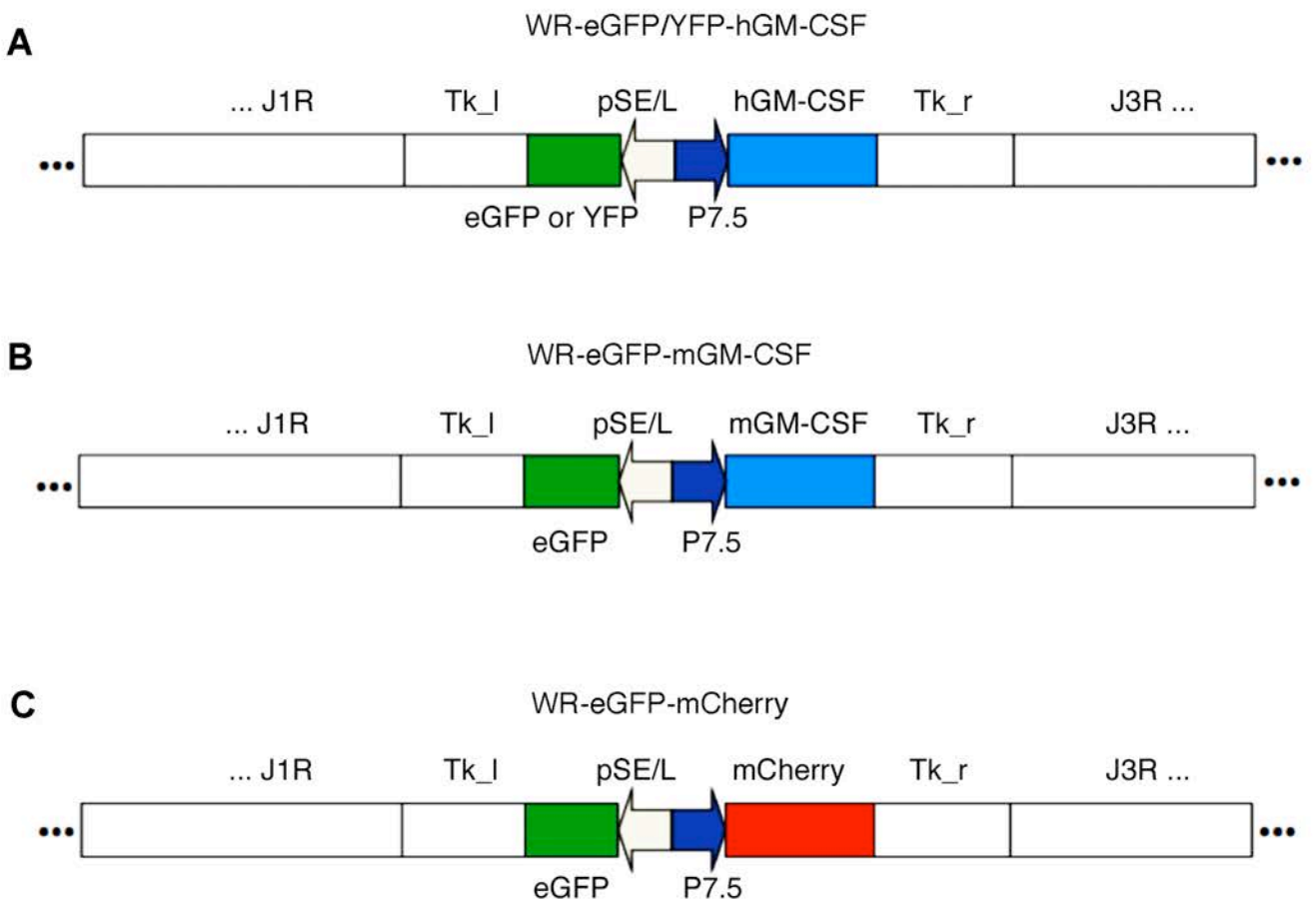

Supplemental Figure 1

Supplemental Figure 1. Three versions of mouse prototypes of JX-594 (mpJX-594) differing by the insertion cassette used to disrupt vaccinia thymidine kinase gene. All viruses were based on the Western Reserve (WR) strain, a mouse-adapted Wyeth strain vaccinia that was isolated through serial passage in mouse brain. WR-TK(-)-eGFP/YFP vaccinia viruses that express transgenes for (**A**) human GM-CSF, (**B**) mouse GM-CSF, or (**C**) mCherry instead of GM-CSF were generated by disrupting the vaccinia thymidine kinase gene (Tk) with an insertion cassette containing eGFP (enhanced green fluorescent protein) or YFP (yellow fluorescent protein) driven by a synthetic early/later promoter (pSel) and human or mouse GM-CSF or mCherry transgene driven by the p7.5 early/late promoter. J1R, gene for virion protein required for morphogenesis; J3R, gene for multifunctional poly-A polymerase subunit, cap methyltransferase, and transcription elongation factor.

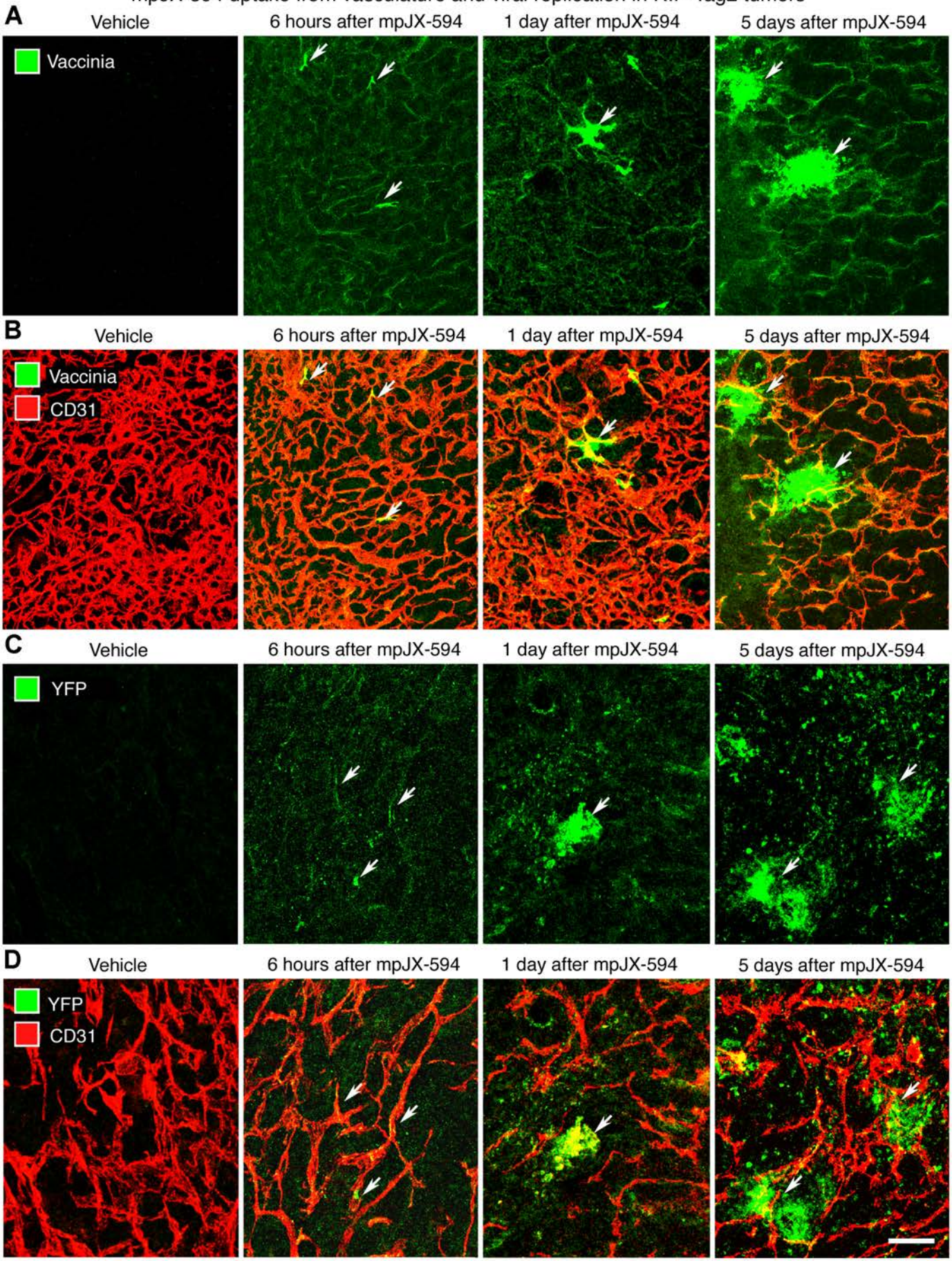

Supplemental Figure 2

Supplemental Figure 2. mpJX-594 uptake from vasculature and replication in RIP-Tag2 tumors. A, B: Confocal micrographs of vaccinia immunoreactivity (green) in RIP-Tag2 tumors. No vaccinia is present after iv injection of vehicle, but 6 hours after mpJX-594, faint vaccinia is uniformly visible in blood vessels (**B**, CD31, red). Some vessels have strong staining (arrows). At 1 day, vaccinia is also located in small groups of cells near tumor vessels (arrow). At 5 days, larger patches of vaccinia are present (arrows). **C, D:** Yellow fluorescent protein (YFP, green) is absent after vehicle, but is visible in tumor vessels (**D**, CD31, red) at 6 hours after mpJX-594 (arrows), and in vessels and extravascular cells (arrows) at 1 and 5 days. Scale bar in D applies to all images: 100 μm in A, B and 50 μm in C, D.

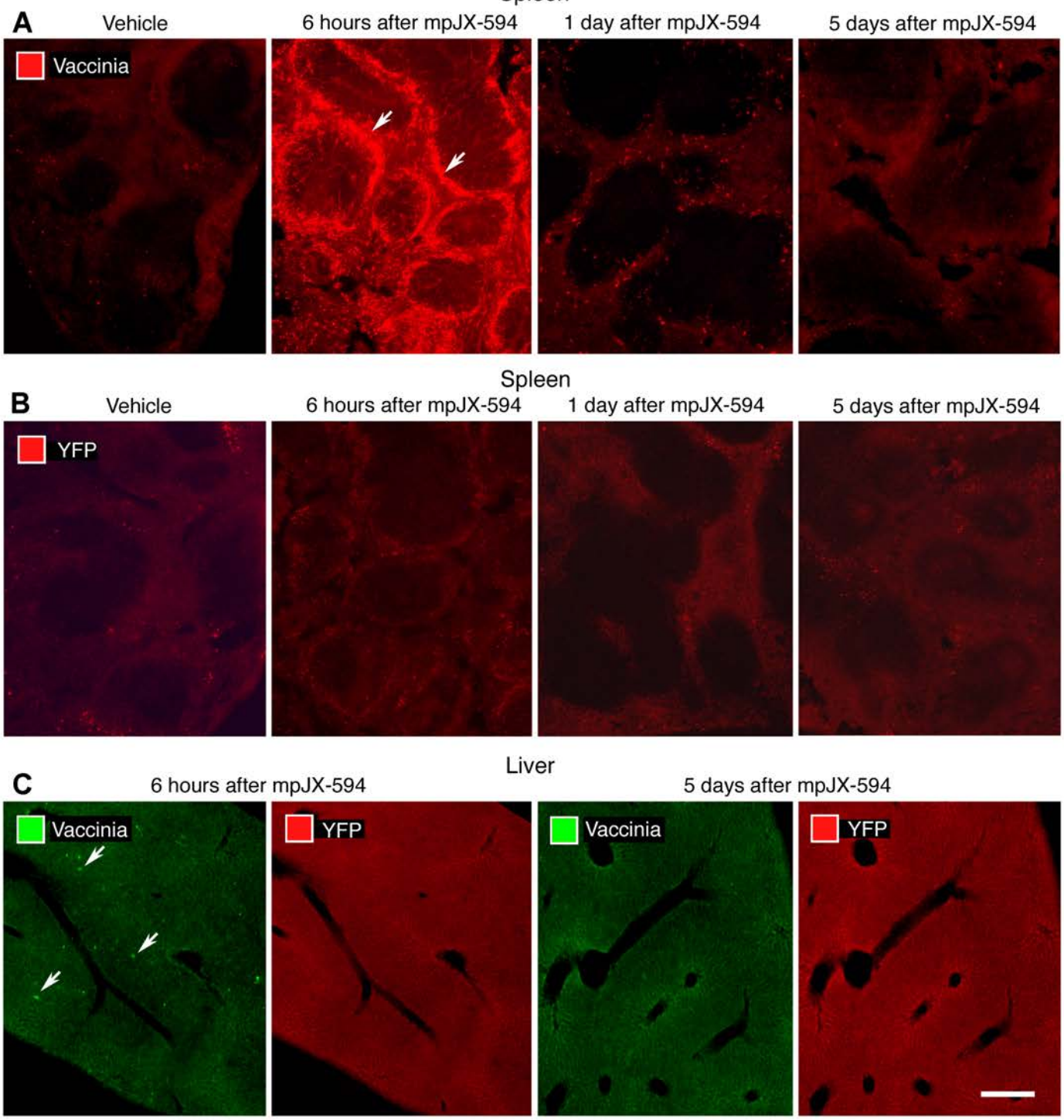

Supplemental Figure 3

Supplemental Figure 3. mpJX-594: transient vaccinia but not YFP in spleen and liver. Confocal micrographs of spleen or liver of RIP-Tag2 mice after iv injection of vehicle or mpJX-594; tissue prepared 6 hours, 1 day, or 5 days later. **A:** Spleen stained for vaccinia immunoreactivity (red). No vaccinia is evident after injection of vehicle as expected, but vaccinia is conspicuous (arrows) in splenic red pulp at 6 hours after mpJX-594, but little or none is present at 1 or 5 days. **B:** Staining of spleen for yellow fluorescent protein (YFP, red) as an indication of mpJX-594 viral replication. No YFP staining is evident at any time point. **C:** Liver stained for vaccinia (green) and YFP (red). Faint vaccinia staining is evident in liver at 6 hours (**C** left, arrows) but not at 5 days (**C** right). No YFP is visible at either time point. Scale bar in C applies to all images: 160 μm.

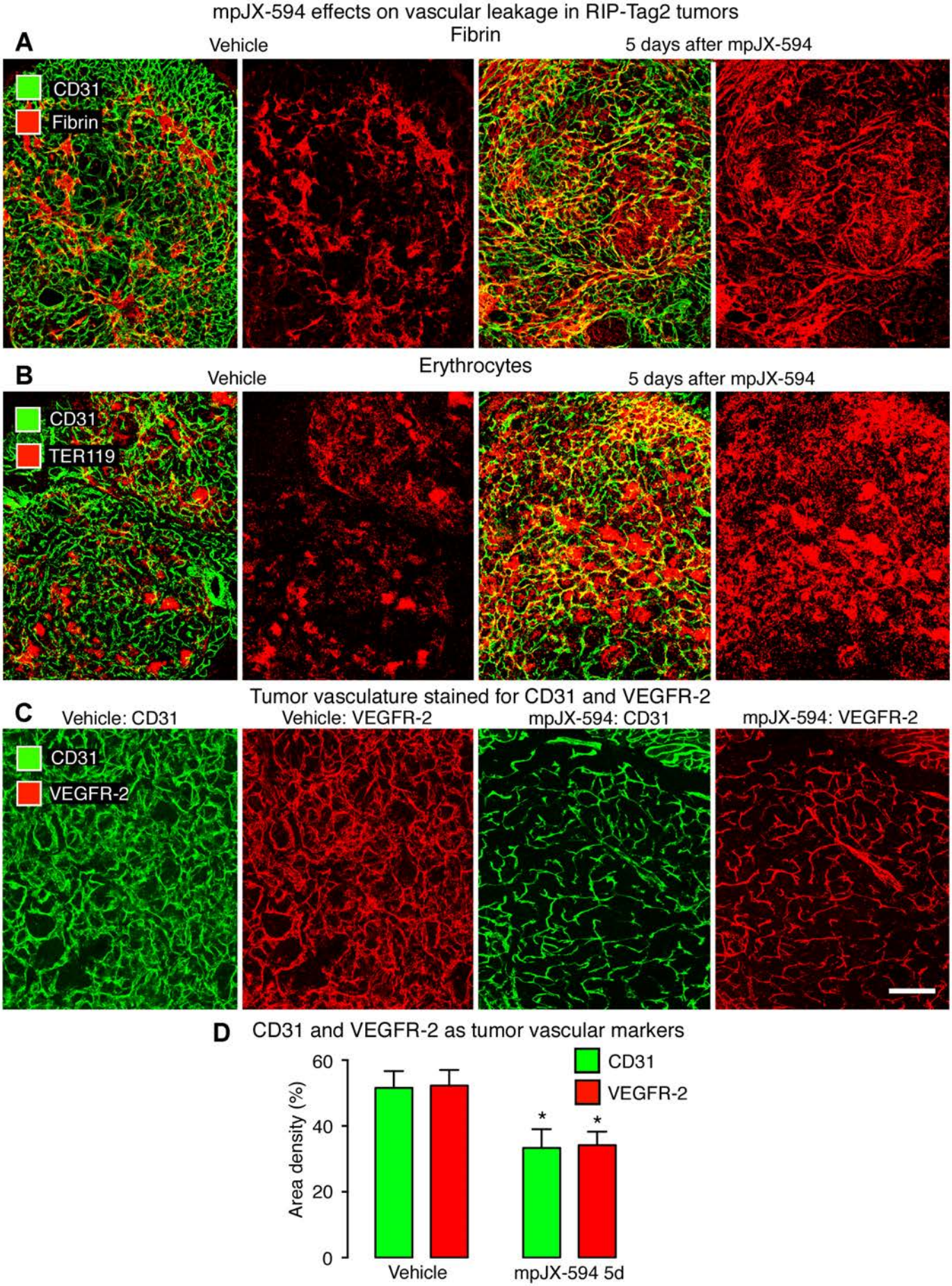

Supplemental Figure 4

Supplemental Figure 4. mpJX-594: effects on extravasation of fibrin and erythrocytes in RIP-Tag2 tumors. **A, B:** Regions of extravasated fibrin/fibrinogen (red, **A**) and erythrocytes (TER119 staining, red, **B**) are scattered in RIP-Tag2 tumors of control (vehicle) mice but are much greater and more widespread at 5 days after mpJX-594. Most erythrocytes in the vehicle-treated tumor are concentrated in blood lakes, which are separate from the vasculature (CD31, green) and are not washed free of blood by vascular perfusion of fixative [Hashizume, 2000 #329]. **C:** Comparison of tumor vasculature co-stained for CD31 and VEGFR-2 at 5 days after iv injection of vehicle or mpJX-594. The tumor vasculature is similar when assessed by CD31 or VEGFR-2. Tumors are highly vascular after vehicle and less vascular after mpJX-594. **D:** Measurements of tumors co-stained for CD31 and VEGFR-2 show similar tumor densities assessed under baseline conditions (vehicle) and similar reductions at 5 days after mpJX-594. ANOVA. *$P < 0.05$ for difference compared to vehicle (n = 5 mice/group). Scale bar in D applies to all images: 200 μm.

Comparison of 3 mpJX-594 variants: limited contribution of GM-CSF to antitumor action (5 days)

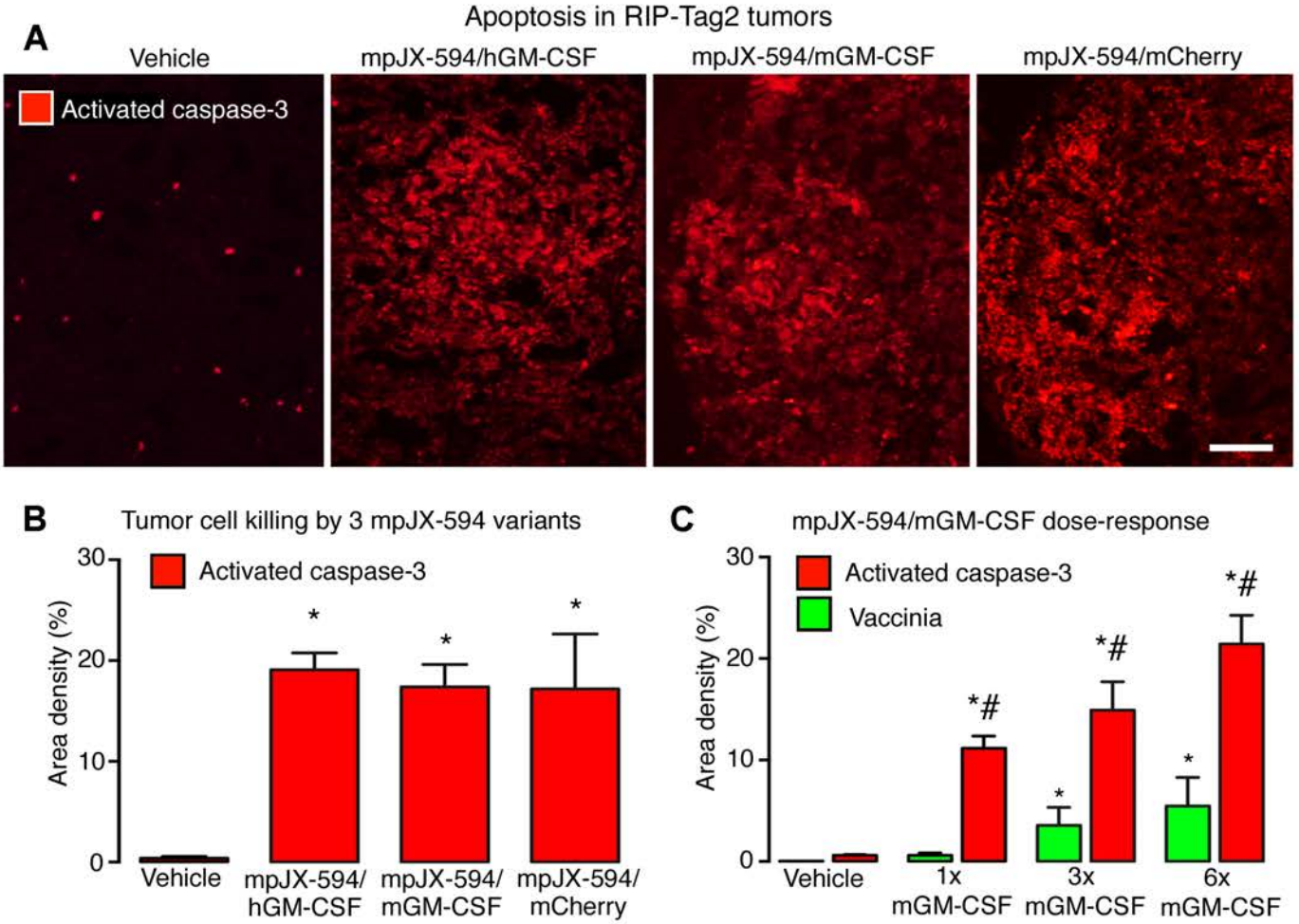

Supplemental Figure 5

Supplemental Figure 5. Antitumor effects of mpJX-594 variants expressing human GM-CSF, mouse GM-CSF, or no GM-CSF and dose-response. A: Confocal micrographs of apoptotic cells (activated caspase-3, red) in tumors of RIP-Tag2 mice at 5 days after iv injection of mpJX-594 variants that express human GM-CSF, mouse GM-CSF, or no GM-CSF (mCherry). **B:** Measurements of activated-casepase-3 staining in tumors show similar increases in apoptotic cells after all three mpJX-594 variants compared to vehicle-treated controls. ANOVA. * $P < 0.05$ compared to vehicle (n = 4-5 mice/group). **C:** Differences in area densities of activated caspase-3 (red) and vaccinia (green) in RIP-Tag2 tumors at 5 days after doses of 1, 3, or 6 times the standard dose (10^7 pfu) of mpJX-594/mGM-CSF. ANOVA. $P < 0.05$ compared to corresponding value for * vehicle or # vaccinia (vehicle, n = 3; 1x mpJX-594, n = 4; 3x mpJX-594, n = 5; 6x mpJX-594, n = 3). Scale bar in A applies to all images: 200 μm.

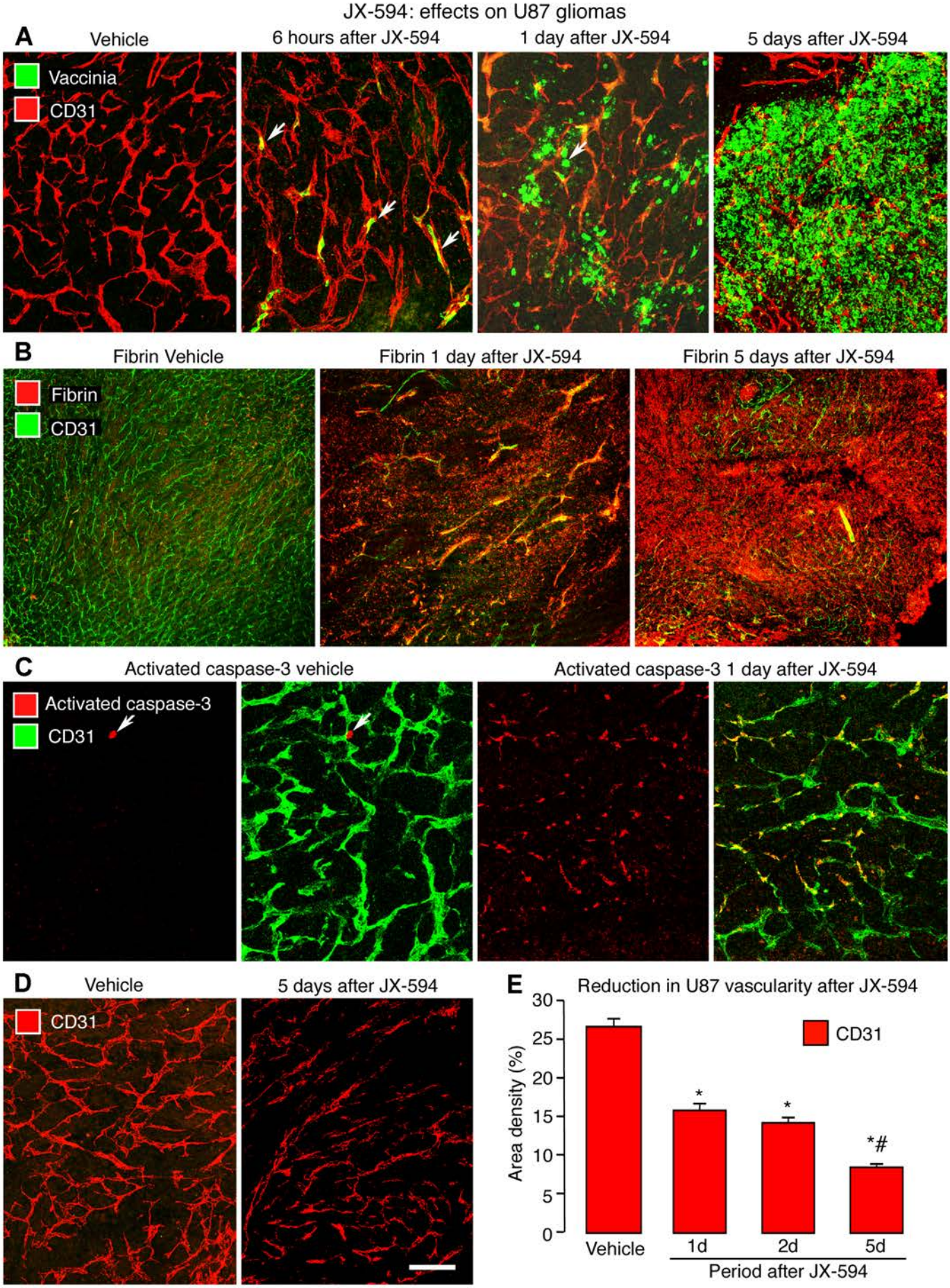

Supplemental Figure 6

Supplemental Figure 6. JX-594: effects on U87 glioma xenografts. A: Confocal micrographs show the amount and distribution of vaccinia staining (green) in and around the vasculature (CD31, red) of human U87 tumor xenografts in nude mice at 6 hours, 1 day, or 5 days after iv injection of JX-594. Control tumor (vehicle) without vaccinia shown for comparison. Arrows point to vaccinia staining in blood vessels. **B:** Little extravasated fibrin (red) in a U87 tumor at baseline compared to conspicuous perivascular fibrin at 1 day and widespread fibrin at 5 days after JX-594. **C:** One apoptotic cell (activated caspase-3, red, arrow) near a blood vessel (CD31, green) in a vehicle-treated U87 tumor compared to numerous apoptotic cells in or near blood vessels in a U87 tumor 1 day after JX-594. **D:** Blood vessels (CD31, red) of U87 tumor at baseline compared to 5 days after JX-594. Tumor vessels are sparse and narrow or fragmented after JX-594. **E:** Reduction of vascularity of U87 tumors from 1 to 5 days after JX-594. ANOVA. $P < 0.05$ for differences compared to * vehicle or to # 2 days or less after JX-594 (n = 5 mice/group). Scale bar in D applies to all images: 100 μm for A, C, D; 400 μm for B.

Sunitinib amplification of mpJX-594 antitumor actions: independence of GM-CSF

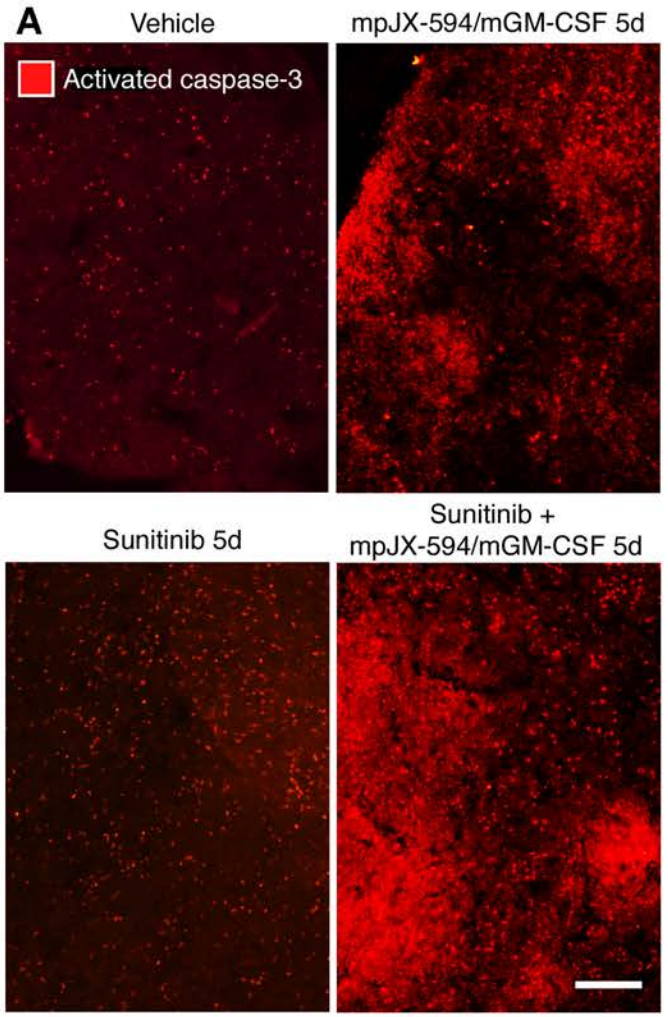

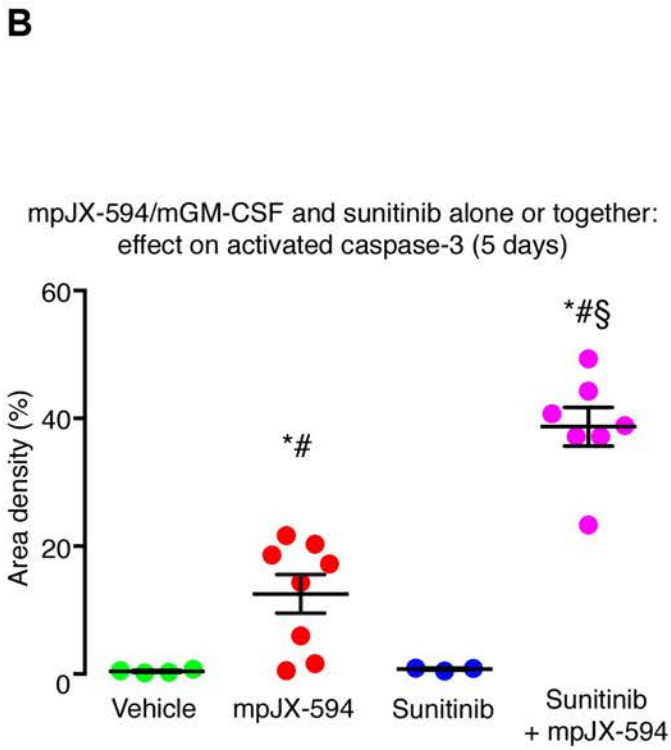

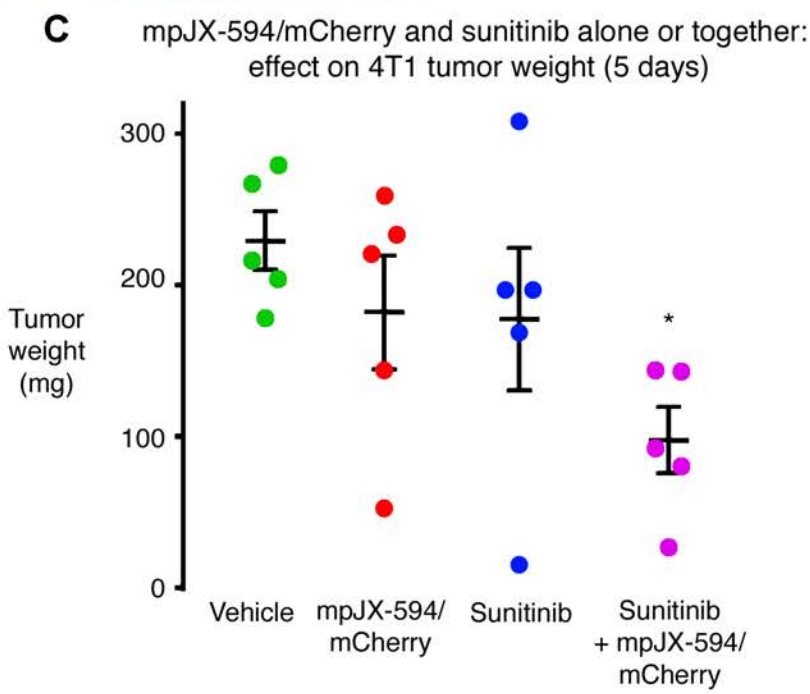

Supplemental Figure 7

Supplemental Figure 7. Sunitinib amplification of mpJX-594 antitumor actions on tumors independent of GM-CSF. A: Confocal micrographs comparing sparse apoptotic cells (activated caspase-3, red) in RIP-Tag2 tumors at 5 days after vehicle or sunitinib with extensive apoptosis after mpJX-594/mGM-CSF (mouse GM-CSF) and even more widespread apoptosis after the virus plus sunitinib. **B:** Measurements of treatment-related differences in activated-caspase-3 staining in tumors from the four groups of mice shown in A. ANOVA. $P < 0.05$ compared to * vehicle, to # sunitinib alone, or to § virus alone (vehicle, n = 4; virus, n = 8; sunitinib, n = 3; virus plus sunitinib, n = 7). **C:** Weight of 4T1 mouse mammary carcinomas implanted subcutaneously in BALB/c mice after treatment with vehicle, mpJX-594/mCherry (no GM-CSF), sunitinib, or virus plus sunitinib over 5 days. One dose of virus was injected iv and daily sunitinib was started on day 0. 4T1 tumors treated with virus plus sunitinib were significantly smaller than the controls. ANOVA. * $P < 0.05$ compared to vehicle (n = 5 mice/group). Scale bar in A: 200 μm.

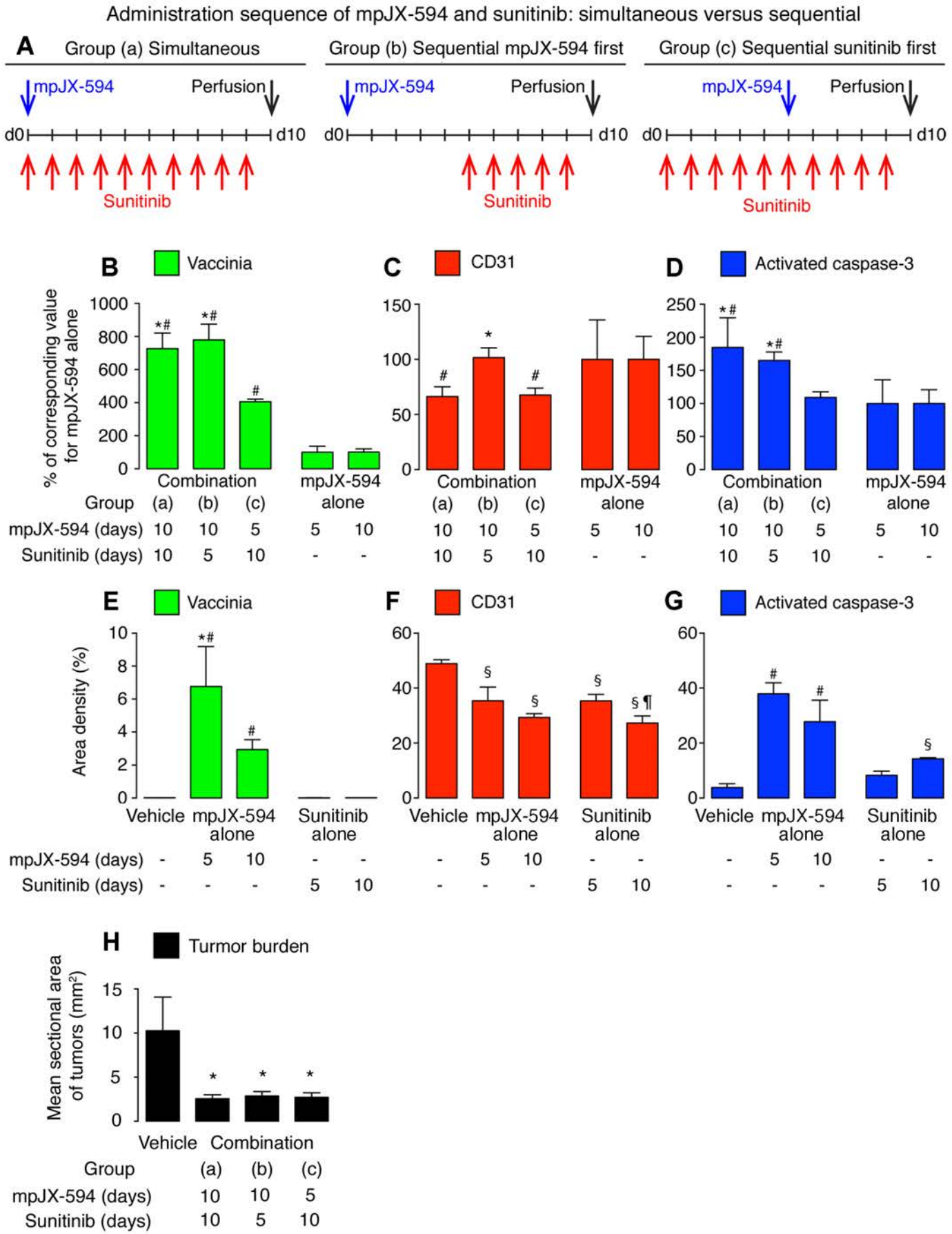

Supplemental Figure 8

Supplemental Figure 8. **mpJX-594 and sunitinib: effects of administration sequence**. **A:** Treatment regimens used to compare sequence of mpJX-594 and sunitinib administration on efficacy in RIP-Tag2 mice: *Simultaneous* (a), *mpJX-594-first* (b), and *Sunitinib-first* (c). **B-D:** Area densities of vaccinia (**B**), CD31 (**C**), and activated caspase-3 (**D**) are expressed as percentages of the corresponding value for mpJX-594 alone for 10 days *(Simultaneous* and *mpJX-594-first*) or 5 days (*Sunitinib-first*). **E-G:** Treatment-related differences in area density of vaccinia (**E**), CD31 (**F**), and activated caspase-3 (**G**) in tumors after vehicle (-/-), mpJX-594 alone, or sunitinib alone for 5 or 10 days. $P < 0.05$ in B-D compared to * *Sunitinib-first* (group c) or to # mpJX-594 alone for 5 or 10 days. $P < 0.05$ in E-G compared to * 10-day mpJX-594 group, # vehicle and sunitinib groups, § vehicle group, or ¶ 5-day sunitinib group. Student's *t*-test comparison of group (b) in panel C and of 10-day mpJX-594 group in panel E to other groups; otherwise ANOVA (n = 4-5 mice/group). **H:** Measurements of tumor burden, assessed as mean sectional areas of RIP-Tag2 tumors in four treatment groups, show smaller values after mpJX-594 plus sunitinib regardless of administration sequence. ANOVA. * $P < 0.05$ compared to vehicle (n = 4-5 mice/group).

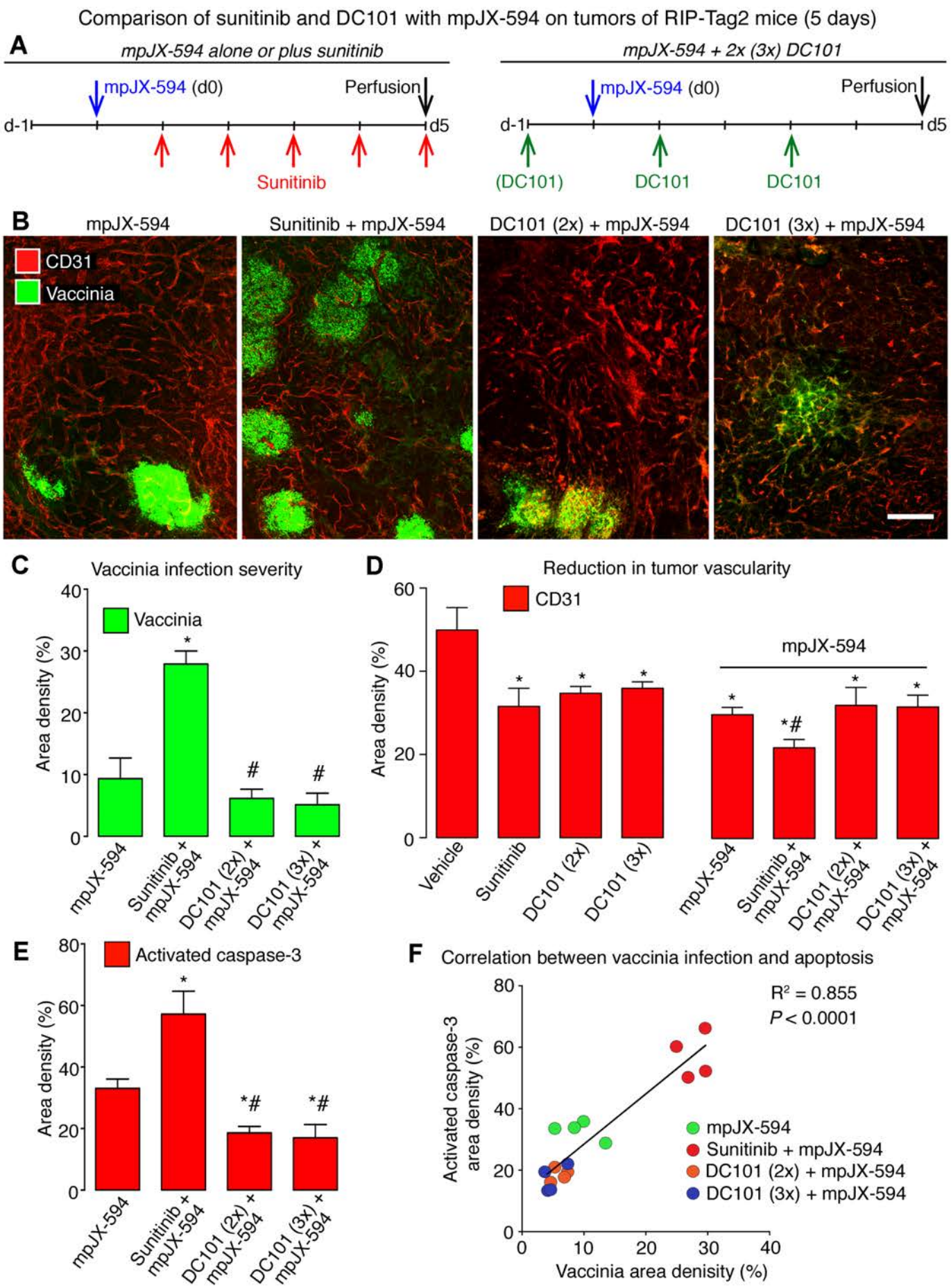

Supplemental Figure 9

Supplemental Figure 9. Sunitinib compared to DC101 in combination with mpJX-594. A: Treatment protocols for administration of sunitinib or DC101 with mpJX-594 to RIP-Tag2 mice over 5 days. mpJX-594 injected iv on day 0. Sunitinib given by gavage daily on days 1 through 5. DC101 given on days 1 and 3 (2x) or as a priming dose on day -1 followed by doses on days 1 and 3 (3x). **B:** Confocal micrographs of tumors show patches of strong vaccinia staining (green) after mpJX-594 alone and more widespread vaccinia after mpJX-594 plus sunitinib. By comparison, vaccinia is weaker after mpJX-594 plus DC101 (2x or 3x). Tumor vessels marked by CD31 (red). **C:** Measurements of vaccinia staining in tumors after mpJX-594 show 3-fold increase after sunitinib but not after DC101. ANOVA. $P < 0.05$ compared to * mpJX-594 alone or to # mpJX-594 plus sunitinib (n = 4 mice/group). **D:** Measurements of tumor vascular density at 5 days after vehicle, sunitinib, or DC101, with or without mpJX-594. Only sunitinib plus mpJX-594 resulted in greater reduction in vascular density than other treatments. $P < 0.05$ compared to * vehicle or # all other groups (n = 3-6 mice/group). **E:** Treatment-related differences in activated caspase-3 in tumors. ANOVA. $P < 0.05$ compared to * mpJX-594 alone or # mpJX-594 plus sunitinib (n = 4 mice/group). **F:** Linear regression shows significant correlation between vaccinia and activated caspase-3 staining in tumors from the four treatment groups with consistently greater staining for activated caspase-3 than vaccinia. Scale bar in B applies to all images: 200 μm.

Amplification of oncolytic vaccinia virus widespread tumor cell killing by sunitinib through multiple mechanisms

Minah Kim, Maximilian Nitschké, Barbara Sennino, Patrizia Murer, Brian J. Schriver, Alexander Bell, Aishwarya Subramanian, Corry E. McDonald, Jiahu Wang, Howard Cha, Marie-Claude Bourgeois-Daigneault, David H. Kirn, John C. Bell, Naomi De Silva, Caroline J. Breitbach and Donald M. McDonald

Supplemental Methods

Tissue preparation, immunohistochemistry, and imaging

Cryostat sections 80-μm in thickness were stained with combinations of two or three primary antibodies (1): (i) vaccinia virus: rabbit anti-vaccinia (1:500, Quartett, V-Biognostics); (ii) yellow fluorescent protein: goat anti-YFP (1:2000, Abcam); (iii) endothelial cells: rat anti-CD31 (clone MEC 13.3; 1:500; BD Pharmingen), hamster anti-CD31 (clone 2H8; 1:500; Pierce), or goat anti-VEGFR-2 (1:500, R&D AF644); (iv) fibrinogen/fibrin: rabbit polyclonal anti-fibrinogen/fibrin (1:2000; Dako); (v) erythrocytes: rat anti-TER119 (1:250, BD Biosciences); (vi) apoptotic cells: rabbit anti-activated caspase-3 (1:1000, R&D Systems); (vii) RIP-Tag2 tumor cells: guinea pig anti-swine insulin (1:100, Dako), or rabbit anti-SV40 T-antigen (1:500, Santa Cruz Biotechnology); (viii) pancreatic acinar cells: rabbit anti-amylase (1:500, Sigma-Aldrich); (ix) immune cells: rat anti-CD45 antibody (1:500, BD Pharmingen) or rat anti-CD8 (1:500, clone YTS169.4, UCSF Monoclonal Antibody Core).

Secondary antibodies were FITC-, Cy3- or Cy5-labeled donkey anti-goat, donkey/goat anti-rabbit, donkey/goat anti-rat, or donkey/goat anti-guinea pig IgG antibody (Jackson ImmunoResearch; all diluted 1:400). Cell nuclei were stained with Vectashield mounting medium containing DAPI (Vector Laboratories).

Measurements of tumor sections

Fractional area (area density) of vaccinia, CD31, activated caspase-3, extravasated microspheres, fibrin, or erythrocytes in digital fluorescence microscopic images of 80-μm sections of tumor was measured as the amount of immunoreactivity above a predetermined fluorescence intensity threshold (1). Tumor invasiveness was measured as the abundance of pancreatic acinar cells (amylase) surrounded by tumor cells (SV40 T-antigen) and expressed as a fraction of tumor area (2).

RIP-Tag2 tumor burden was calculated as the sum of areas of tumors visible in a montage of digital images of a pancreas section from each mouse (5x objective, 1x Optovar, section dimensions 1,920 by 2,560 μm) (2). Mean tumor area was also calculated (Supplemental Figure 7H).

Liver micrometastases were identified in images of 80-μm-thick sections of liver of RIP-Tag2 mice at age 17 weeks by the presence of two or more adjacent SV40 T-antigen-positive cells (3). Incidence was expressed as proportion of mice with liver micrometastases. Number of micrometastases was expressed per 10 mm^2 of liver section (3).

Flow cytometry

RIP-Tag2 mice were anesthetized, blood was removed by vascular perfusion of PBS for 2 minutes, and tumors were removed, weighed and digested in collagenase II and IV solution (625U/ml, Gibco) with DNase (60U/ml, Roche) for 30 minutes at 37°C, and erythrocytes were lysed. Total cells per tumor were counted with a Muse Cell Analyzer (Millipore Sigma, Billerica, MA). Cells were stained with anti-CD45-APC-Cy7, anti-CD3e-PE-Cy7 or anti-CD3e-Alexa 647,

anti-CD4-Alexa 647, anti-CD8-PerCP-Cy5.5 or anti-CD8-Alexa 700 (all BioLegend). Viable cells were identified by live-dead staining (Zombie Yellow, BioLegend). Some preparations were then permeabilized (Foxp3 staining buffer set, eBioscience) and stained with anti-Foxp3-eFluor 450 (eBioscience) for regulatory T-cells, with anti-granzyme B-FITC (Biolegend) for $CD8^+$ T-cell activation, or with non-specific control immunoglobulin of the same isotype (mouse IgG1, both BioLegend) as a control. Cells were sorted by FACS (BD Fortessa) and analyzed with FlowJo software (8.8.6 and X). All staining and washing steps were performed in the presence of GolgiPlug (1:1000, BD Biosciences). Cells per mg tumor were calculated from total acquired cells (gated by FSC/SSC, excluding debris).

1. Inai T, Mancuso M, Hashizume H, Baffert F, Haskell A, Baluk P, Hu-Lowe DD, Shalinsky DR, Thurston G, Yancopoulos GD, McDonald DM. Inhibition of vascular endothelial growth factor (VEGF) signaling in cancer causes loss of endothelial fenestrations, regression of tumor vessels, and appearance of basement membrane ghosts. Am J Pathol 2004;165:35-52.
2. Sennino B, Ishiguro-Oonuma T, Wei Y, Naylor RM, Williamson CW, Bhagwandin V, Tabruyn SP, You WK, Chapman HA, Christensen JG, Aftab DT, McDonald DM. Suppression of tumor invasion and metastasis by concurrent inhibition of c-Met and VEGF signaling in pancreatic neuroendocrine tumors. Cancer Discov 2012;2:270-87.
3. Moen I, Gebre M, Alonso-Camino V, Chen D, Epstein D, McDonald DM. Anti-metastatic action of FAK inhibitor OXA-11 in combination with VEGFR-2 signaling blockade in pancreatic neuroendocrine tumors. Clin Exp Metastasis 2015;32:799-817.
4. Hashizume H, Baluk P, Morikawa S, McLean JW, Thurston G, Roberge S, Jain RK, McDonald DM. Openings between defective endothelial cells explain tumor vessel leakiness. Am J Pathol 2000;156:1363-80.